6-1-1997

An Experimental determination of freeplay and its effect on modal complexity and damping

Timothy S. Merle

AN EXPERIMENTAL DETERMINATION OF FREEPLAY AND ITS EFFECT ON MODAL COMPLEXITY AND DAMPING

by

Timothy S. Merle

A Thesis Submitted
in
Partial Fulfillment
of the
Requirements for the

MASTER OF SCIENCE
IN

Mechanical Enginering

Approved by:

Professor _____
Dr. Kevin Kochersberger

Professor _____
Dr. Josef Török

Professor _____
Dr.Wayne Walter

Professor _____
Dr. Charles W. Haines

Department Head

DEPARTMENT OF MECHANICAL ENGINEERING
COLLEGE OF ENGINEERING
ROCHESTER INSTITUTE OF TECHNOLOGY

JUNE 1997

Abstract:

This experiment is designed to address the effects of joint related nonlinearities on system parameters. Specifically, the effects of freeplay on the natural frequency, damping, and modal complexity. Many modal analysis techniques assume a system exhibits linear properties that are time invariant. Large structures are commonly constructed with several pinned and bolted joints and these joints can lead to gap and frictional-type nonlinearities. Joint nonlinearities will result in exaggerated damping estimates and complex time-varying mode shapes. These characteristics will result in incorrect modal parameter estimation when estimation assumes linearity.

The experiment's intent is to examine nonlinearities and indicate methods of estimating the amount of nonlinearity and the degree of looseness, of a joint, associated with the nonlinearity. A real system, constructed of masses, springs, and viscoelastic components will be tested to arrive at these results.

The results of this experiment indicated that it is possible to identify freeplay in the system. In addition to this, a new method of determining a system's degree of nonlinearity was developed.

TABLE OF CONTENTS

List of Figures: page

page

List of Tables: page

1 Introduction:

This experiment is designed to address the effects of joint related nonlinearities on system parameters. Specifically, the effects of freeplay on the natural frequency, damping, and modal complexity. The experiment will indicate methods of estimating the amount of nonlinearity and the degree of looseness, of a joint, associated with the nonlinearity.

Many modal analysis techniques assume a system exhibits linear properties that are time invariant. This is most often for reasons of simplicity. Most nonlinear analysis involves complex math which is time consuming and requires expensive software. Real structures experience variations to their structural parameters over time due to evolutionary and event driven property changes as well as changes due to movement of components which lead to nonlinear system behavior. Sources of nonlinearities include pinned and bolted joints, these joints can induce gap and frictional-type nonlinearities. Joint nonlinearities will result in exaggerated damping estimates and complex time-varying mode shapes. These characteristics will result in incorrect modal parameter estimation when linearity is assumed.

Large structures such as air and space crafts are subject to these nonlinearities due to their relatively large number of joint interfaces. A critical maintenance step for any reusable launch vehicle is the detection and identification of structural faults and impending failure prior to each launch. These vehicles under go extreme amounts of stress and strain during launch, flight, and ascent [2]. These loads are detrimental to the

fastened joints causing sources of nonlinearities to appear, such as cracks, elongation, and changes in the contact pressure of the joints.

An investigation into the effects of freeplay was undertaken. The investigation was on a real system consisting of three masses and two springs. Known quantities of freeplay could be introduced into the system in two different locations. System response was recorded for a number of combinations of power, freeplay size, and freeplay location.

The parameters were extracted using a circle fit technique and studied for trends which could be related to the freeplay. The intent of the experiment was to determine if parameter trends could identify freeplay in the system. It was hoped that the parameters could be manipulated to identify the amount and location of the freeplay.

It was found that while freeplay was identifiable in the system, the exact amount of freeplay was indeterminable from the results of the freeplay analysis. It was possible, though, to quantify the amount of freeplay on an arbitrary scale based on the freeplay range used in the test.

1.1 Literature Review:

A major part of any dynamic analysis is extracting the modal parameters, the modal analysis, of the system. Any number of methods can be employed to do this and typically data from an experiment is fit in either the frequency domain or the time domain. The frequency response functions (FRF) are used while working in the frequency domain and the Inverse Fourier Transform of the FRF is used while in the time domain. An FRF represents the response amplitude for any given frequency and the Inverse Fourier Transform relies on the Impulse Response Function which represents the system's response to a single impulse.

A system's response contains all the information necessary to determine the modal parameters of a system. The parameters are often extracted from the data using any one of a number of curve fitting techniques. One method of curve fitting involves the fit of rational polynomials to a systems response characteristics. There is traditionally a great deal of difficulty curve fitting polynomials in rational fraction form. The solution equations are ill-conditioned and therefore are difficult if not impossible to solve. Richardson and Formenti [13] present a new method of parameter extraction which overcomes many of the numerical analysis problems associated with the least squares error parameter estimation. The new method utilizes a special property of FRFs. This property is that the real part of the FRF for positive frequency values can be folded around the origin, resulting in the FRF for negative frequencies. This allows representation of the FRF in terms of linear combinations of orthogonal polynomials. The

orthogonal polynomials are able to be solved for their unknown coefficients which can then be used to determine the unknown coefficients of the ordinary polynomials. This results in a fairly easy numerically stable method of extracting system parameters.

For the experiment of this thesis it was determined that for parameter extraction, the Circle-Fit-Method would best suit the system. This method utilizes the fact that when plotted in the Nyquist plane the real and imaginary data points of the FRF result in an almost perfect circle. The points of the circle are naturally magnified around the natural frequency. This allows close examination of the points near the natural frequency. The modal parameters can easily and accurately be extracted from the Nyquist plot [4]. A detailed description of this method can be viewed in section 4.

These methods of parameter extraction are useful in determining the response of the most simplest of structures to more complex structures, such as a space structure. Moon and Li [12] performed an experiment on a 16 bay pin jointed truss. The purpose of the study was to investigate the effects of an actual pin jointed truss on the dynamic response of a mutibay space truss. The experiment results demonstrated that when excited by a sinusoid, the system exhibited chaotic-like vibrations. It was believed that small gaps in the joints created nonlinearities, resulting in chaotic vibrations. In an attempt to control the chaotic vibrations, a cable was added to the truss to induce a compressive preload on the structure. The experiment showed that modal frequencies of the real system were considerably lower than ideal values for the truss and also indicated that the

internal compressive load may partially reduce the chaotic behavior under low forcing levels.

One of the problems with experimentally determining the characteristics of a space truss is the size of the structure, therefore it is common to scale the truss down to a manageable size. When performing an experimental analysis of a scaled space structure, it is important to consider two factors: the tolerances in the joints may be impossible to scale, due to their already quite high tolerances, and that there will be preloads on the truss, due to gravity. A study performed by Hsu, Griffin, and Bielak [6] addressed this problem. Using several different analytical approaches it was determined that the amplitude of the response will be multivalued over a range of excitation values. It proved difficult to get repeatable results since the structure tends to settle into different patterns of response depending on subtle changes in the loading conditions. The study also showed that under some conditions the preloads could significantly effect the system response.

Gaul, Lenz, and Sachau [5] also experimented with a space truss. The goal of their experiment was to implement active damping through contact pressure control in the joints. The joint pressure was controlled by piezoelectric discs at the joints. A finite element model of the structure was examined once using linear assumptions and again using nonlinear estimates. Then the response of a single pressure controlled joint was examined. The results of the finite element analysis was combined with the results of the actual joint to simulate the trusses response with active damping present. The damping

capacity of the structure with active damping proved to be significantly larger than with fixed contact pressure.

In dynamic analysis it is common to represent the friction experienced in contacting surfaces as a point contact coulomb damper. This idealization is acceptable if there is gross slip at the contact, usually the result of small normal loads. This will lead to inaccurate results if, as in the case of the previous space truss, the normal loads are high. When the loads are high, one part of the friction interface may be slipping while other parts remain stuck (friction stick). Memq, Bielak and Griffin [10,11] developed a new approach for calculating the harmonic response of a structure constrained by a friction contact subject to high normal loads. This study resulted in an explanation of the friction behavior which match the experimental results.

The space truss experiments both showed a significant contribution to the system response made by the freeplay, or looseness in the joints. This showed a need for further examination of the effects and predictability of freeplay.

An examination of the effects of freeplay and a method of determining the amount of freeplay present was performed by Alexander, Noah and Franck [1]. Their study was of a cantilever beam type system with a gap. The system was designed such that a cantilevered beam end would contact a 'stop' at one extreme of its cycle with certain excitation levels. The distance between the still beam and the 'stop' is referred to as the gap. The research involved analytical and experimental investigations. The response of the system was determined analytically using two methods. One method involved a finite

elements program and another using an equivalent single-degree-of-freedom closed-form solution, the closed-form was able to be obtained by utilizing the piecewise linearity of the system. The analytical results were used to predict the system parameters. These parameters could be used to calculate the gap size, given the system response. Their results showed a consistency between the predicted and actual system parameters.

Masri [8] also investigated freeplay using the cantilever beam type system. The motion of the mechanical model exhibited a jump phenomena similar to that shown by the solution of Duffing's equation. It was determined that the initial conditions played a significant role in determining the system parameters. Masri found that the amplification curves of the system strongly depended on whether the frequency was increasing or decreasing. This agrees with the implications of Duffing's equation. Duffing's equation states that for a softening spring, decreasing excitation frequency will result in a higher amplitude FRF than increasing excitation frequency (the opposite is true for a hardening spring). Also, a closed-form analytical solution was derived for the steady-state motion of the system. The results of the analysis were confirmed through experimental measurements.

A study of a slightly more complex beam structure was performed by Chattopadhyay and Saxena [3]. Their experiment involved having a gap on both sides of the beam and the gap was able to be located anywhere along the beam. The nonlinearities modified the results from a linear model and exhibited complex responses such as jump phenomena, subharmonic oscillations, quasiperiodic response, and chaotic vibrations.

The motion of the beam was found to be quite sensitive to the gap dimension as well as excitation frequency. The experiment showed that the distortion of the response curves, from linear curves, became more severe as the gap was moved closer to the free end of the beam. The curves showed multivalued responses, also noted by Hsu, Griffin, and Bielak in their study of scaled space structures.

Several of the papers reviewed mentioned 'jump phenomena'. The jump phenomena results in an asymmetry around the resonant frequency, it is an indication that nonlinear spring behavior is taking place. The nonlinear spring may be in the form of a cubicly hardening or softening spring or the presence of coulomb friction. The jump phenomena is described by the Duffing equation, the equation of motion of a mass on a nonlinear cubic hardening or softening spring subject to harmonic excitation [9].

The papers reviewed give some indications of what one can expect from a system containing freeplay. The freeplay often results in response characteristics exhibiting the jump phenomena. The results of these papers indicate that there is a need for further examination of freeplay and its effects on various systems.

2 Theory:

Complex multi-degree-of-freedom systems, subject to joint freeplay or other nonlinearities can be investigated using simpler systems. Initially a two-degree-of-freedom system was proposed so that a simulation of the system, using Simulink® could be generated. Problems developed in the simulation in that the available computers did not have enough memory to acquire the frequency resolution necessary for the model with freeplay present. Equation development for the two-degree-of-freedom system is presented for the purpose of the simulation. The two-degree-of-freedom was expanded to a three-degree-of-freedom system to induce complexity to allow the experiment to be applicable to larger more complex systems.

2.1 Equation Development - Linear Dynamics:

The system parameters were calculated for a two mass, one spring setup. A model of this system is seen in figure 2.1-1.

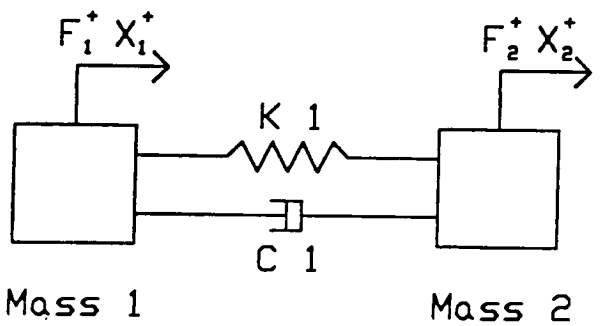

Figure 2.1-1

There are two basic equations of motion to describe this system; they are:

$$\begin{aligned} M_1\ddot{x}_1 + C_1(\dot{x}_1 - \dot{x}_2) + K_1(x_1 - x_2) &= F \\ M_2\ddot{x}_2 + C_1(\dot{x}_2 - \dot{x}_1) + K_1(x_2 - x_1) &= F \end{aligned} \tag{2.1}$$

These can be written in matrix form:

$$[M]\{\ddot{x}\} + [C]\{\dot{x}\} + [K]\{x\} = \{f(t)\} \tag{2.2}$$

This can be expanded to be:

$$\begin{bmatrix} M_1 & 0 \\ 0 & M_2 \end{bmatrix}\begin{Bmatrix} \ddot{x}_1 \\ \ddot{x}_2 \end{Bmatrix} + \begin{bmatrix} C_1 & -C_1 \\ -C_1 & C_1 \end{bmatrix}\begin{Bmatrix} \dot{x}_1 \\ \dot{x}_2 \end{Bmatrix} + \begin{bmatrix} K_1 & -K_1 \\ -K_1 & K_1 \end{bmatrix}\begin{Bmatrix} x_1 \\ x_2 \end{Bmatrix} = \begin{Bmatrix} F_1 \\ F_2 \end{Bmatrix} \tag{2.3}$$

The input force is assumed to have the form:

$$F = Fe^{i\omega t} \tag{2.4}$$

The output can be assumed to have the same form:

$$\begin{aligned} x &= \mathrm{X}e^{i\omega t} \\ \dot{x} &= i\omega \mathrm{X}e^{i\omega t} \\ \ddot{x} &= -\omega^2 \mathrm{X}e^{i\omega t} \end{aligned} \tag{2.5}$$

Substituting equations (2.4) and (2.5) into equation (2.3) results in:

$$\left(-\omega^2\begin{bmatrix} M_1 & 0 \\ 0 & M_2 \end{bmatrix} + i\omega\begin{bmatrix} C_1 & -C_1 \\ -C_1 & C_1 \end{bmatrix} + \begin{bmatrix} K_1 & -K_1 \\ -K_1 & K_1 \end{bmatrix}\right)\begin{Bmatrix} \mathrm{X}_1 \\ \mathrm{X}_2 \end{Bmatrix} e^{i\omega t} = \begin{Bmatrix} F_1 \\ F_2 \end{Bmatrix} e^{i\omega t} \tag{2.6}$$

Assuming the damping coefficient, C, is negligible and considering that the force is applied only to mass 1, equation (2.6) reduces to:

$$\left(-\omega^2\begin{bmatrix} M_1 & 0 \\ 0 & M_2 \end{bmatrix}+\begin{bmatrix} K_1 & -K_1 \\ -K_1 & K_1 \end{bmatrix}\right)\begin{Bmatrix} X_1 \\ X_2 \end{Bmatrix}e^{i\omega t}=\begin{Bmatrix} F_1 \\ 0 \end{Bmatrix}e^{i\omega t} \tag{2.7}$$

To obtain the natural frequency the homogeneous part of the equation is solved. The force is assumed to be equal to zero. This will result in the matrix equation:

$$\begin{bmatrix} -\omega M_1+K & -K \\ -K & -\omega M_2+K \end{bmatrix}\begin{Bmatrix} X_1 \\ X_2 \end{Bmatrix}=0 \tag{2.8}$$

To arrive at a nontrivial solution of matrix equation (2.8), the determinant of the matrix must be equal to zero. The determinant of the matrix results in the quadratic equation:

$$\begin{aligned} &\text{for } M_1 = M_2 = M \\ &\lambda^2 M^2 - \lambda 2MK = 0 \\ &\text{where } \lambda = \omega^2 \end{aligned} \tag{2.9}$$

For demonstration purposes, K = 20,000 lbs/in and a target value of ω_n = 785.4 rad/sec was selected. When substituted into equation (2.9), these values result in a mass of .0648 lbs sec^2/in^2, an equivalent weight of 25.04 lbs.

For the three mass, two spring system modeled in figure 2.1-2,

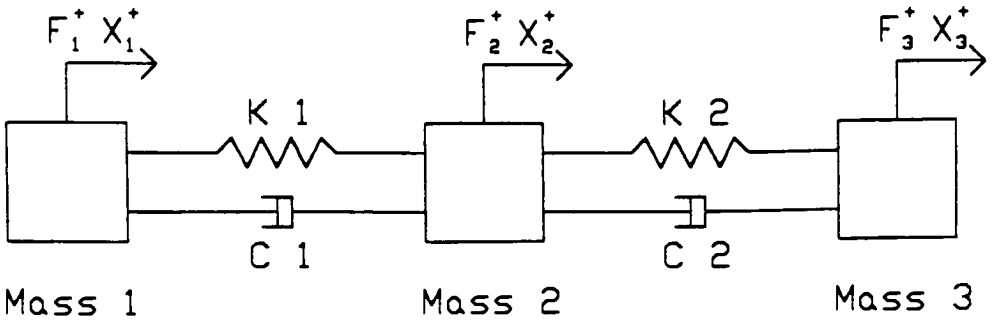

Figure 2.1-2

The system equations are:

$$\begin{aligned} &M_1\ddot{x}_1 + C_1(\dot{x}_1 - \dot{x}_2) + K_1(x_1 - x_2) = F \\ &M_2\ddot{x}_2 + C_1(\dot{x}_2 - \dot{x}_1) + C_2(\dot{x}_2 - \dot{x}_3) + K_1(x_2 - x_1) + K_2(x_2 - x_3) = 0 \\ &M_3\ddot{x}_3 + C_2(\dot{x}_3 - \dot{x}_2) + K_2(x_3 - x_2) = 0 \end{aligned} \tag{2.10}$$

With the force applied only to mass 1 and assuming the damping coefficient, C, is negligible, equation (2.10) can be expanded to matrix format:

$$\begin{bmatrix} M_1 & 0 & 0 \\ 0 & M_2 & 0 \\ 0 & 0 & M_3 \end{bmatrix} \begin{Bmatrix} \ddot{x}_1 \\ \ddot{x}_2 \\ \ddot{x}_3 \end{Bmatrix} + \begin{bmatrix} K_1 & -K_1 & 0 \\ -K_1 & K_1 + K_2 & -K_2 \\ 0 & -K_2 & K_2 \end{bmatrix} \begin{Bmatrix} x \\ x \\ x \end{Bmatrix} = \begin{Bmatrix} F \\ 0 \\ 0 \end{Bmatrix} \tag{2.11}$$

Assuming the same input and output as in equations (2.4) and (2.5) respectively, and solving the homogeneous part of equation (2.11) results in:

$$\begin{bmatrix} -\omega^2 M_1 + K_1 & -K_1 & 0 \\ -K_1 & -\omega^2 M_2 + K_1 + K_2 & -K_2 \\ 0 & -K_2 & -\omega^2 M_3 + K_2 \end{bmatrix} \begin{Bmatrix} X_1 \\ X_2 \\ X_3 \end{Bmatrix} = 0 \qquad (2.12)$$

To arrive at a nontrivial solution of matrix equation (2.7), the determinant of the matrix must be equal to zero. The determinant of the matrix results in the polynomial equation:

$$\begin{aligned} &-\lambda^3 M^3 + \lambda^2 4M^2 K - \lambda 3MK^2 = 0 \\ &\lambda = \omega^2 \end{aligned} \qquad (2.13)$$

Where, for demonstration purposes:

$$\begin{aligned} &M_1 = M_2 = M_3 = .0647 \, lbs \cdot \sec^2/_{in} \\ &K_1 = K_2 = 20{,}000 \, lbs/_{in} \end{aligned} \qquad (2.14)$$

Substituting the values of (2.14) into (2.13) and solving for λ, results in a rigid body mode of 0 Hz, a second mode frequency of 88.48 Hz, and a third mode frequency of 153.28 Hz.

Equation (2.12) in the standard form of an eigenvalue problem is:

$$\begin{aligned} &M_1 = M_2 = M_3 = M \\ &K_1 = K_2 = K \\ &\lambda = \omega^2 \end{aligned}$$

$$\begin{bmatrix} K/M & -K/M & 0 \\ -K/M & 2K/M & -K/M \\ 0 & -K/M & K/M \end{bmatrix} \begin{Bmatrix} X_1 \\ X_2 \\ X_3 \end{Bmatrix} - \lambda \begin{bmatrix} 1 & 0 & 0 \\ 0 & 1 & 0 \\ 0 & 0 & 1 \end{bmatrix} \begin{Bmatrix} X_1 \\ X_2 \\ X_3 \end{Bmatrix} = \begin{Bmatrix} 0 \\ 0 \\ 0 \end{Bmatrix} \tag{2.15}$$

To solve for the eigenvectors, the eigenvalues (λ) are substituted into one of the system equations along with the values given in (2.14). For example the solution for the second eigenvector proceeds as follows:

$$\lambda = 309E3$$

The first equation:

$$\begin{aligned} (K/M)X_1 - (K/M)X_2 - \lambda X_1 &= 0 \\ (309E3 - 309E3)X_1 - (309E3)X_2 &= 0 \\ X_2 &= 0 \end{aligned} \tag{2.16}$$

The second equation:

$$\begin{aligned} -(K/M)X_1 + (2K/M)X_2 - (K/M)X_3 - \lambda X_2 &= 0 \\ (-309E3)X_1 - (309E3)X_3 &= 0 \\ -X_3 &= X_1 \end{aligned}$$

The second eigenvector is:

$$\phi_2 = \begin{Bmatrix} X_1 \\ X_2 \\ X_3 \end{Bmatrix} = \begin{Bmatrix} 1 \\ 0 \\ -1 \end{Bmatrix} \tag{2.17}$$

The third eigenvector is:

$$\phi_3 = \begin{Bmatrix} X_1 \\ X_2 \\ X_3 \end{Bmatrix} = \begin{Bmatrix} -1 \\ 2 \\ -1 \end{Bmatrix} \tag{2.18}$$

The first eigenvector, the rigid body mode, is:

$$\phi_1 = \begin{Bmatrix} X_1 \\ X_2 \\ X_3 \end{Bmatrix} = \begin{Bmatrix} 1 \\ 1 \\ 1 \end{Bmatrix} \tag{2.19}$$

To mass normalize the eigenvectors the diagonalized mass matrix is used. This is done by pre- and post-multiplying the mass matrix by a matrix of mode shapes seen below:

$$[\Phi] = \begin{bmatrix} 1 & 1 & -1 \\ 1 & 0 & 2 \\ 1 & -1 & -1 \end{bmatrix} \tag{2.20}$$

Using the previously found mass, the mass matrix:

$$[M] = \begin{bmatrix} .0647 & 0 & 0 \\ 0 & .0647 & 0 \\ 0 & 0 & .0647 \end{bmatrix} \tag{2.21}$$

To diagonalize the mass matrix, the mass matrix is pre- and post-multiplied by the eigenvector:

$$\begin{bmatrix} \ddots & & \\ & m_{ii} & \\ & & \ddots \end{bmatrix} = [\Phi]^T [M][\Phi] \tag{2.22}$$

This results in:

$$\begin{bmatrix} \ddots & & \\ & m_{ii} & \\ & & \ddots \end{bmatrix} = \begin{bmatrix} .1941 & 0 & 0 \\ 0 & .1294 & 0 \\ 0 & 0 & .3882 \end{bmatrix} \tag{2.23}$$

To mass normalize the eigenvectors:

$$\hat{\phi}_i = \frac{1}{\sqrt{m_{ii}}} \phi_i \tag{2.24}$$

The mass normalized vectors are:

$$\hat{\phi}_1 = \begin{Bmatrix} 2.27 \\ 2.27 \\ 2.27 \end{Bmatrix} \tag{2.25}$$

$$\hat{\phi}_2 = \begin{Bmatrix} 2.78 \\ 0 \\ -2.78 \end{Bmatrix} \tag{2.26}$$

$$\hat{\phi}_3 = \begin{Bmatrix} -1.6 \\ 3.2 \\ -1.6 \end{Bmatrix} \tag{2.27}$$

To obtain the equation of a frequency response function (or FRF as will be used throughout) a new variable Y is introduced:

$$[\phi]\{Y\} = \{X\} \tag{2.28}$$

where {Y} consists of the modal coordinates Y_1 And Y_2

Substituting (2.28) into equation (2.6):

$$\left(-\omega^2[M]+i\omega[C]+[K]\right)[\phi]\begin{Bmatrix}Y_1\\Y_2\end{Bmatrix}e^{i\omega t}=\begin{Bmatrix}F_1\\0\end{Bmatrix}e^{i\omega t} \tag{2.29}$$

pre-multiplying by $[\phi]^T$ results in:

$$[\phi]^T\left(-\omega^2[M]+i\omega[C]+[K]\right)[\phi]\begin{Bmatrix}Y_1\\Y_2\end{Bmatrix}e^{i\omega t}=[\phi]^T\begin{Bmatrix}F_1\\0\end{Bmatrix}e^{i\omega t}$$

Which because of orthogonality of the eigenvectors results in:

$$\left(-\omega^2\begin{bmatrix}\ddots & & \\ & M & \\ & & \ddots\end{bmatrix}+i\omega\begin{bmatrix}\ddots & & \\ & C & \\ & & \ddots\end{bmatrix}+\begin{bmatrix}\ddots & & \\ & K & \\ & & \ddots\end{bmatrix}\right)\begin{Bmatrix}Y_1\\Y_2\end{Bmatrix}e^{i\omega t}=[\phi]^T\begin{Bmatrix}F_1\\0\end{Bmatrix}e^{i\omega t} \tag{2.30}$$

With the diagonal matrices it becomes easy to solve for Y:

$$\begin{Bmatrix}Y_1\\Y_2\end{Bmatrix}=\left(-\omega^2\begin{bmatrix}\ddots & & \\ & M & \\ & & \ddots\end{bmatrix}+i\omega\begin{bmatrix}\ddots & & \\ & C & \\ & & \ddots\end{bmatrix}+\begin{bmatrix}\ddots & & \\ & K & \\ & & \ddots\end{bmatrix}\right)^{-1}[\phi]^T\begin{Bmatrix}F_1\\0\end{Bmatrix} \tag{2.31}$$

To obtain the X vector, [ϕ] is multiplied through (as seen in equation (2.28)):

$$\begin{Bmatrix}X_1\\X_2\end{Bmatrix}=[\phi]\left(-\omega^2\begin{bmatrix}\ddots & & \\ & M & \\ & & \ddots\end{bmatrix}+i\omega\begin{bmatrix}\ddots & & \\ & C & \\ & & \ddots\end{bmatrix}+\begin{bmatrix}\ddots & & \\ & K & \\ & & \ddots\end{bmatrix}\right)^{-1}[\phi]^T\begin{Bmatrix}F_1\\0\end{Bmatrix} \tag{2.32}$$

Writing out the mode vectors and solving for X_1 results in:

$$X_1 = \left(\phi_{11}\left(\frac{1}{-\omega^2 m_{11} + i\omega c_{11} + k_{11}} \right) + \phi_{12}\left(\frac{1}{-\omega^2 m_{22} + i\omega c_{22} + k_{22}} \right) \right) \begin{bmatrix} \phi_{11} & \phi_{21} \\ \phi_{12} & \phi_{22} \end{bmatrix} \begin{Bmatrix} F_1 \\ 0 \end{Bmatrix}$$

$$X_1 = \left(\phi_{11}\left(\frac{1}{-\omega^2 m_{11} + i\omega c_{11} + k_{11}} \right) + \phi_{12}\left(\frac{1}{-\omega^2 m_{22} + i\omega c_{22} + k_{22}} \right) \right) F_1 \tag{2.33}$$

For a force at the *j*th degree of freedom and the response of the *r*th mode at the *i*th degree of freedom equation (2.33) can be expressed as:

$$\frac{X_i}{F_j} = \sum_{r=1}^{n} \left(\frac{\phi_{ir}\phi_{jr}}{-\omega^2 m_{rr} + i\omega c_{rr} + k_{rr}} \right) \tag{2.34}$$

Using the mass normalized eigenvector results in the simpler form:

$$\frac{X_i}{F_j} = \sum_{r=1}^{n} \left(\frac{\hat{\phi}_{ir}\hat{\phi}_{jr}}{-\omega^2 + i2\varsigma\omega_r\omega + \omega_r^2} \right) \tag{2.35}$$

Substituting the values found earlier for the mass normalized eigenvectors and natural frequencies and an arbitrary value for ζ, (.001), a plot of equation (2.35) will result in the FRF seen below, figure 2.1-3.

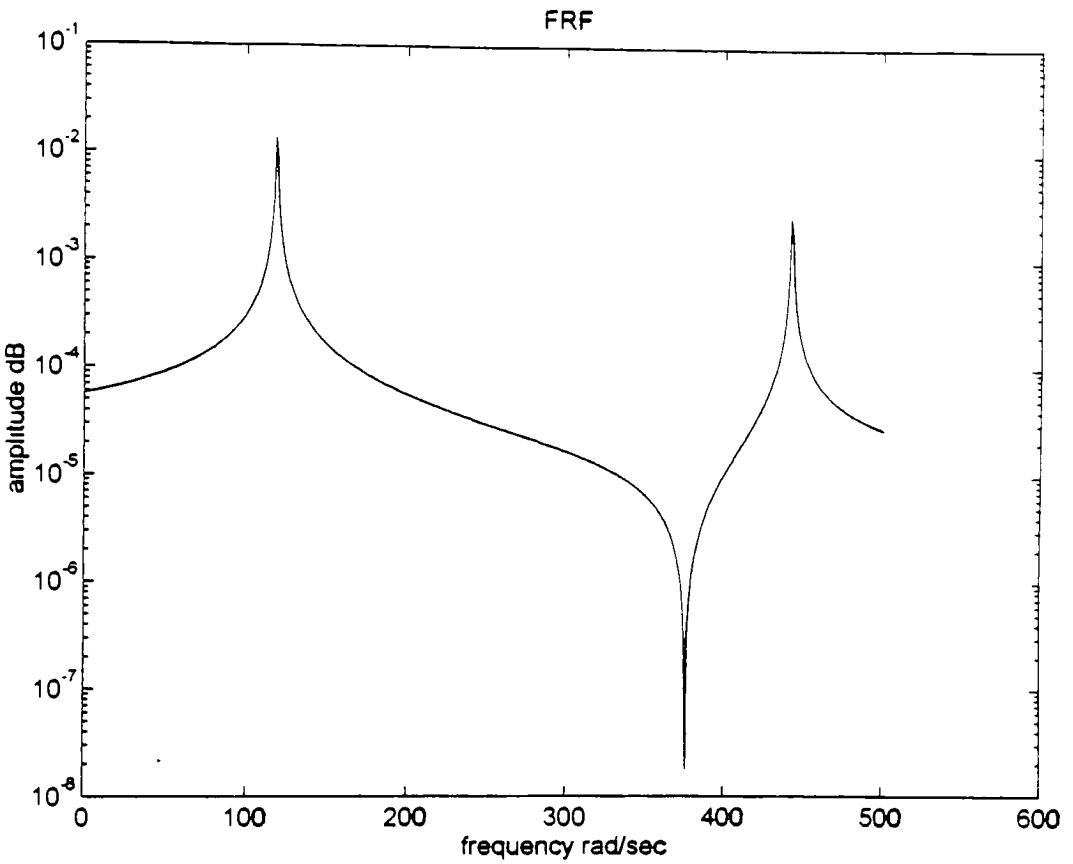

Figure 2.1-3 FRF curve

2.2 Parameter Extraction of Measured Data for Linear Systems; Circle Fitting:

Typically, a dynamic system is tested for the purpose of extracting its modal parameters; the extraction can be performed using any number of methods. A Nyquist, or circle, plot is an effective method of viewing a systems frequency response characteristics and extracting the modal parameters of natural frequency, damping, and residue. The Nyquist plot is a plot of the real verses imaginary response data points of a harmonic system, with each data point corresponding to a particular frequency. An example of a single-degree-of-freedom (SDOF) Nyquist plot can be seen in Figure 2.2-1 (while ω_n would be unknown at this point it is shown here for demonstration purposes).

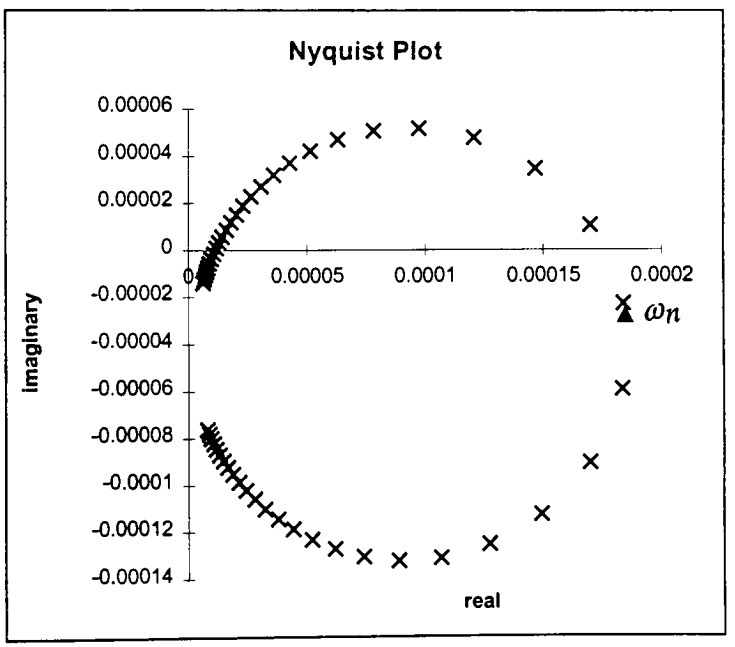

Figure 2.2-1 Nyquist Plot

It can be noted that only about 15 of the data points, the points closest to the resonant frequency (ω_n), are clearly identifiable; the other points are closely bunched

together. This focus on the area of resonance is what makes the Nyquist plot so effective in terms of parameter extraction [4].

The following equations will support the fact that a plot of the real versus imaginary data points will result in a circle.

First start with the basic system equation:

$$M\ddot{x} + C\dot{x} + Kx = F \tag{2.36}$$

Recall the assumed input (2.4) and output (2.5) forms:

$$F = Fe^{i\omega t}$$

$$x = \mathrm{X}e^{i\omega t}$$
$$\dot{x} = i\omega \mathrm{X}e^{i\omega t}$$
$$\ddot{x} = -\omega^2 \mathrm{X}e^{i\omega t}$$

Substituting (2.4) and (2.5) into (2.36) results in:

$$(-\omega^2 M + i\omega C + K)\mathrm{X}e^{i\omega t} = Fe^{i\omega t}$$
$$-\omega^2 M + i\omega C + K = \frac{F}{\mathrm{X}}$$

Which can be arranged to give the receptance FRF of the form:

$$\frac{1}{(K - \omega^2 M) + i\omega C} = \frac{\mathrm{X}}{F} \tag{2.37}$$

This is modified to the mobility FRF form:

$$\dot{X}e^{i\omega t} = i\omega X e^{i\omega t}$$
$$\frac{i\omega}{(K-\omega^2 M)+i\omega C} = \frac{\dot{X}}{F} \tag{2.38}$$

Multiplying by the complex conjugate and separating the result into its real and imaginary components:

$$\frac{\omega^2 C + i\omega(K-\omega^2 M)}{(K-\omega^2 M)^2+(\omega C)^2} = \frac{\dot{X}}{F}$$
$$\frac{\omega^2 C}{(K-\omega^2 M)^2+(\omega C)^2} = \text{real} = (re) \tag{2.39}$$
$$\frac{\omega(K-\omega^2 M)}{(K-\omega^2 M)^2+(\omega C)^2} = \text{imaginary} = (im)$$

Now let $U = \left(re - \frac{1}{2C}\right)$ and $V = im$

The claim that plots of the real and the imaginary data points result in a circle is now supported by:

$$U^2 + V^2 = Radius^2$$
$$\frac{((K-\omega^2 M)^2+(\omega C)^2)^2}{4C^2((K-\omega^2 M)^2+(\omega C)^2)^2} = \left(\frac{1}{2C}\right)^2 \tag{2.40}$$
$$\frac{1}{4C} = \frac{1}{4C}$$

Therefore a plot of:

$$(\text{real data} - A)^2 + (\text{imaginary data} - B)^2 = (\text{radius})^2 \tag{2.41}$$

will result in a circle with center at (A,B) and a radius of (radius); the radius is equal to the residue (modal amplitude).

Using a least squares iterative method to solve equation (2.41) for A, B, and the radius will result in a circle that is a best fit curve to the data points. An example of this can be seen in Figure 2.2-2.

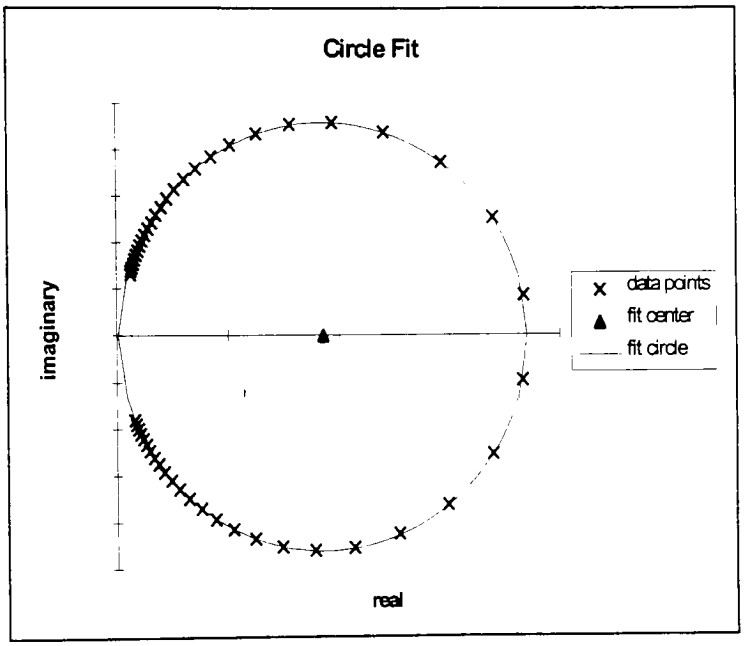

Figure 2.2-2 Nyquist plot with fit circle

Figure 2.2-2 is a typical plot for a SDOF system. A multi-degree-of -freedom (MDOF) system will plot as many circles as there are modes; Figure 2.2-3 is an example of the Nyquist plot of a two-degree-of-freedom system.

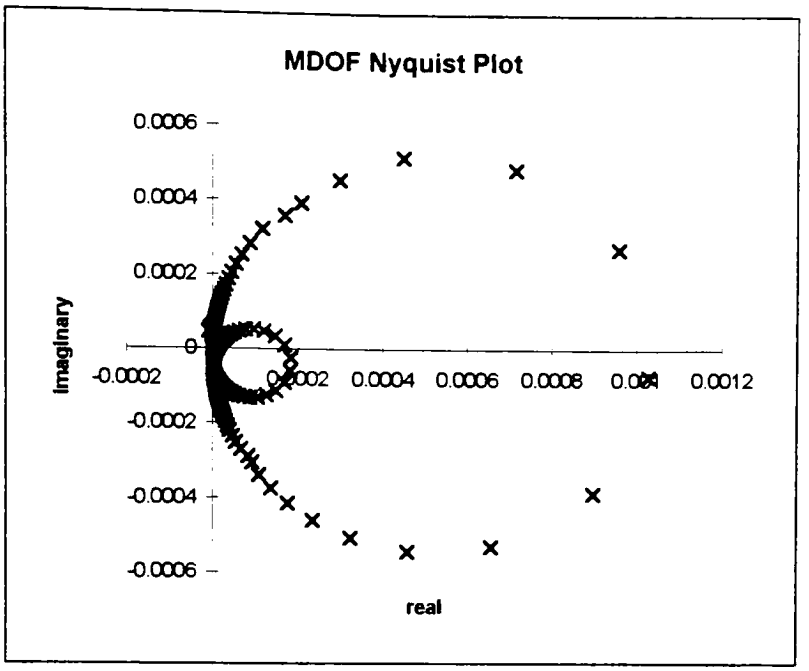

Figure 2.2-3 Nyquist plot showing two modes

The MDOF system can be treated as a SDOF system, if only a small range of frequencies, near the natural frequency, is used when extracting the parameters for each mode. This is because, near resonance, the behavior of most systems is dominated by a single mode. The sum effect of the other modes, (the residual), can be treated as a complex constant which shifts the location of the center of the Nyquist plot [4]. The shift is found by solving for the modal constant. Through manipulation of the measured and 'fit' data, the natural frequency, damping, and the residue of the mode can be determined. The circle fit procedure for extracting the system parameters from the circle is reviewed in Section 3 and used on test data in Section 5..

2.3 Nonlinear Dynamics:

A typical linear FRF would display a degree of symmetry around a vertical line drawn through the natural frequency [4]. A nonlinear system can display FRFs similar to those of Figure 2.3-1.

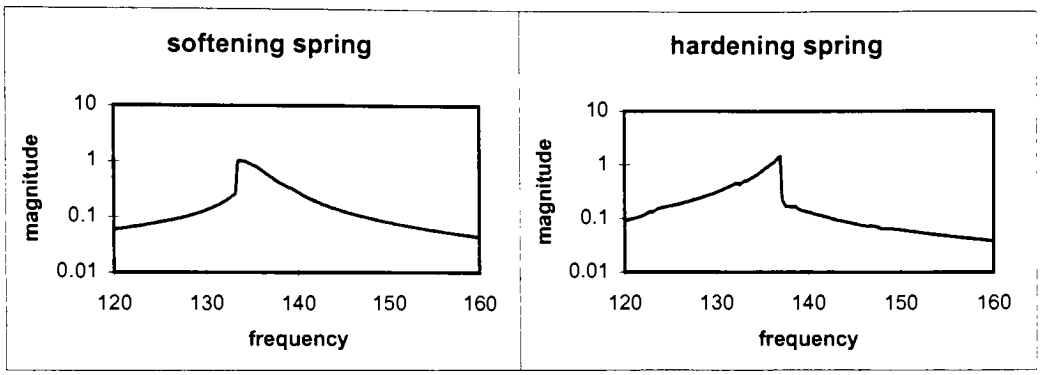

Figure 2.3-1 (a) example FRF of softening spring, (b) hardening spring

The sharp rise or fall seen in Figure 2.3-1 is known as the "jump" phenomena. The jump phenomena can result in a jump on the order of magnitude over a matter of only a couple of frequency bins [9]. The jump is not limited to as drastic a jump as seen in Figure 2.3-1, it can be a small amount of asymmetry around the resonant frequency.

Presence of the jump phenomena indicates a system operating with a hardening or softening spring. The hardening or softening spring phenomena can be represented by a system containing coulomb friction, or caused by a spring with cubic stiffness. The cubic stiffness can give the appearance of either a hardening or softening spring while the coulomb friction will tend to give the appearance of a softening spring [9].

The Duffing equation describes the motion of a system containing a nonlinear cubic hardening or softening spring subject to harmonic excitation [9].

The Duffing equation is:

$$F = M\ddot{x} + C\dot{x} + Kx \pm \beta x^3 \tag{2.42}$$

which is the basic equation of motion with the addition of the cubic term (βx^3), where β is the stiffening factor of the cubic spring. This equation shows that the effects of cubic stiffness is directly related to the distance $(x)^3$ traveled by the spring.

When coulomb friction is present, the equation of motion is:

$$F = M\ddot{x} + C\dot{x} + Kx + \mu N \tag{2.43}$$

Where μ is the coefficient of friction and N is the normal force experienced at the friction point.

A system containing both cubic stiffness and coulomb friction would result in the equation of motion:

$$F - \mu N = M\ddot{x} + C\dot{x} + Kx \pm \beta x^3 \tag{2.44}$$

3 Curve fitting procedure:

Once the frequency response has been recorded, as real and imaginary data, a procedure must be performed on the data to obtain the system parameters. There are several methods to extract this data. It was determined that a circle-fit analysis would be best for the system in question. These are the five basic steps to performing a circle-fit analysis, they will each be discussed later:

1. select points to use in the analysis
2. fit circle to data
3. locate natural frequency
4. calculate damping estimates
5. determine the residue

Following is a brief discussion on how the previously mentioned steps are performed.

Step 1:

Not all of the data collected will be of use to the analysis, some of the data will be too close to each other to be discernible and other data will be too close to other modes. It is up to the person performing the analysis to determine which data points will be used. This can be done by arbitrarily picking a fixed number of points to either side of the suspected resonant frequency or by forming a Nyquist plot of the mobility data and hand picking the data points that will be used for the analysis. The latter method may be better, because the operator can eliminate suspect data points. The points chosen should

encompass 270° of a circle if possible and should definitely cover 180°, also there should be no less than 6 data points used [4].

Step 2:

The next step is to fit a curve to the selected data points. This can be done any number of ways, in this case it was completed using a least squares method which minimized the distance each data point was from the circle. A more accurate method would be to minimize the distance from where each data point is to where it should be on the fit circle. The latter method is fairly complex and the difference in results can be quite small and therefore insignificant, so it was deemed unnecessary for this experiment. Upon completing this step, the center, radius and error of the fit circle should be known.

Step 3:

Finding the resonant frequency accurately is important because the damping estimates and residual term are dependent on the its location. The circle plot can be analyzed to give the natural frequency based on data point locations. Figure 3-1 shows a typical circle plot with two angles identified (the a or b subscript indicate after or before the natural frequency, respectively).

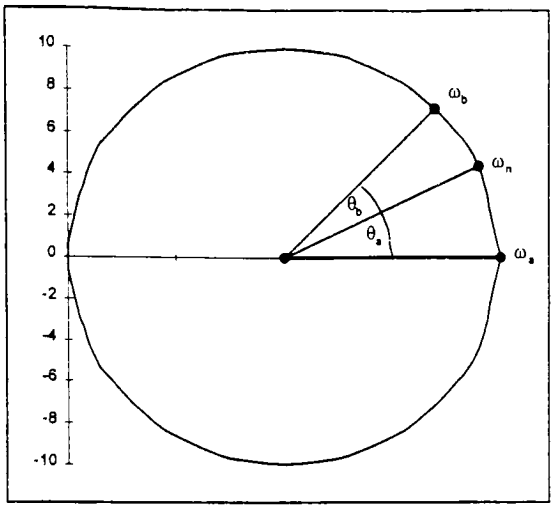

Figure 3-1 Sample circle fit.

The angle θ represents the angle between data points, the point where this angle's rate of change is the maximum is the location of the natural frequency; this is shown below.

Each angle θ can be represented by the following equation [4]:

$$\tan\left(\theta/2\right) = imaginary/real$$

Then:

$$\tan\left(\theta/2\right) = \frac{1-(\omega/\omega_n)^2}{2\zeta\omega/\omega_n} \tag{3.1}$$

which rearranges to:

$$\omega^2 = \omega_n^2\left(1 - 2\zeta\omega/\omega_n \tan\left(\theta/2\right)\right)$$

When differentiated with respect to θ.

$$d\omega^2/d\theta = (-\zeta\omega\omega_n)\left(1+\left(1-\left(\frac{\omega}{\omega_n}\right)^2\right)^2 \Big/ 2\zeta\omega/\omega_n\right) \tag{3.2}$$

This represents the incremental change in frequency as θ changes.

Setting the derivative of this equal to zero represents a maximum rate of change of frequency.

$$d/d\omega\left(d\omega^2/d\theta\right) = 0 \tag{3.3}$$

This is satisfied when $\omega = \omega_n$:

$$d\omega^2/d\theta = \left(-\zeta\omega_n{}^2\right)(1+0)$$

This means that the natural frequency is found at the largest spacing of FRF data points in the Nyquist plot. For linear frequency increments the natural frequency can be found to within 10% of the frequency increments [4].

Step 4:

Refer to the sample curve fit in Figure 3-1 for step 4.

Recall (3.1):

$$\tan\left(\theta/2\right) = {}^{imaginary}/_{real}$$

$$\tan\left(\theta/2\right) = \frac{1-(\omega/\omega_n)^2}{2\zeta\omega/\omega_n} \tag{3.1}$$

If ω is equal to points ω_b and ω_a for points before and after the natural frequency (ω_n) respectively:

$$\tan\left(\theta_b/2\right) = \frac{1-(\omega_b/\omega_n)^2}{2\zeta\omega_b/\omega_n}$$

$$\tan\left(\theta_a/2\right) = \frac{(\omega_a/\omega_n)^2-1}{2\zeta\omega_a/\omega_n} \tag{3.4}$$

When solved for ζ, the damping estimate is:

$$\zeta = \frac{(\omega_a{}^2 - \omega_b{}^2)}{2\omega_n(\omega_a \tan(\theta_a/2) + (\omega_b \tan(\theta_b/2)} \tag{3.5}$$

Equation (3.3) is used to solve for the damping estimates. where ω_a is any frequency located above ω_n, ω_b is any frequency located below ω_n. The angle θ_a is the angle between the ω_n and ω_a, and θ_b is the angle between the ω_n and ω_b. For successive values

of ω_a and ω_b, Equation (3.5) is solved over the entire range of data points selected in step one.

This will result in a range of values for the damping. If the standard deviation of the damping estimates is less than 5%, then the average of these values will be an accurate estimate of the system damping [4]. For a non-linear system the values will tend to deviate more than this. If this proves to be the case, then a surface plot of all the points may be more useful to the analysis.

For step 5 refer to Figure 3-2 of a sample circle fit.

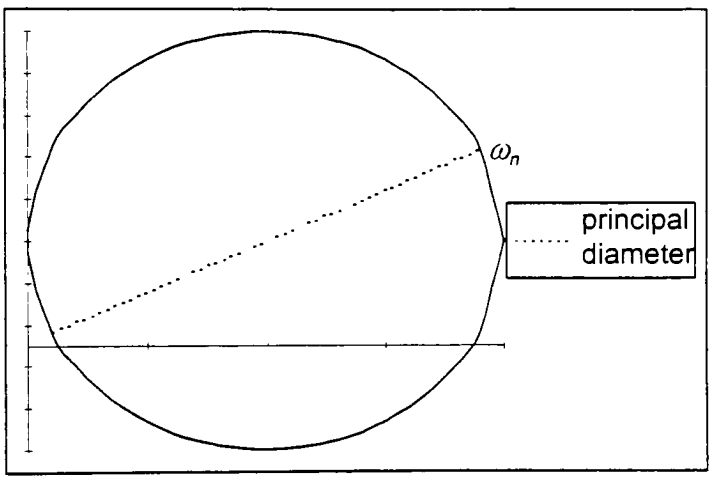

Figure 3.2 Sample circle fit.

Step 5:

Finally the residue is found. This is simply done by determining the distance of a line drawn from the origin to the point location of the natural frequency and the orientation of the line with respect to the real axis. This complex number is the residue [7].

4 Experimental setup and procedure:

The experimental setup consisted of masses of approximately 25 lbs each and springs of approximately 20,000 lbs/in each. The springs were made of 1 inch aluminum tubes, 12 inches long, with holes milled into them to reduce stiffness. Once the springs were completed their stiffness was measured to be approximately 20,000 lb/in. The size of the mass was calculated such that a two mass, one spring system (the model of this can be seen in Figure 2.1-1 in Section 2.1) would resonate at an arbitrary frequency of approximately 125 Hz (the calculations for this are also shown in Section 2.1). The masses were hung from a wooden structure through the use of elastic cords. The two mass system reacted well to experimental pre-runs which led to the determination that a third mass could be added which would provide enough complexity to allow this system to be related to larger systems.

The final three mass, two spring system is pictured in Figure 4-1.

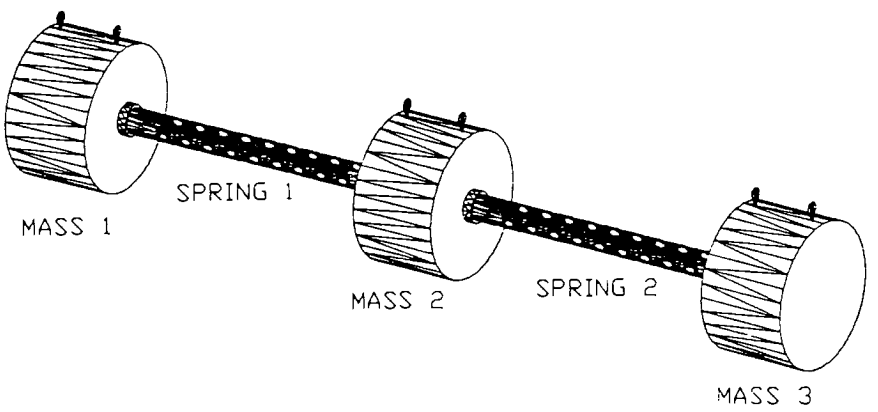

Figure 4-1

Each spring was hard mounted to a mass on one side and connected to the other mass through a mechanism which allowed known quantities of freeplay to be induced into the system. The first freeplay mechanism employed is shown in Figure 4-2.

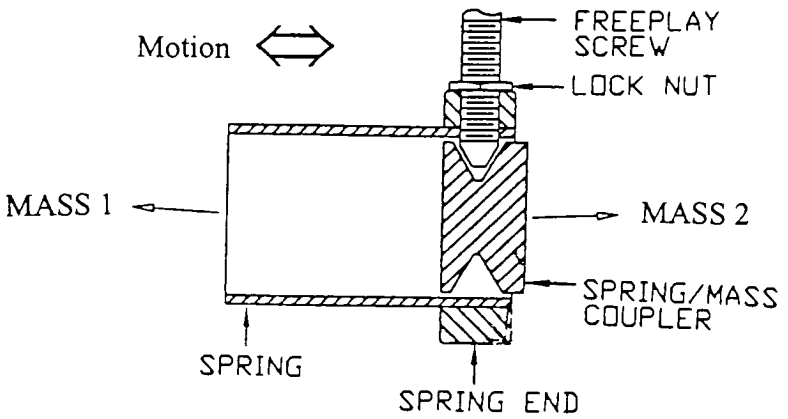

Figure 4-2

The spring/mass coupler is bolted through its center to the center of the mass (this is implied in Figure 4-1). This setup used screws to adjust the freeplay. By turning the screw in or out a known distance, the freeplay between the screw end and the spring end could be calculated. This method seems great on paper but proved less than adequate in practice. The tolerances between the screws and tapped holes were not tight enough to allow the freeplay to be accurately repeated, also different tensions on the lock nut would have noticeable effects on the system response. The freeplay mechanism needed to be completely redesigned.

The new freeplay mechanism used shims to regulate the freeplay. The shim mechanism is shown in Figure 4-3.

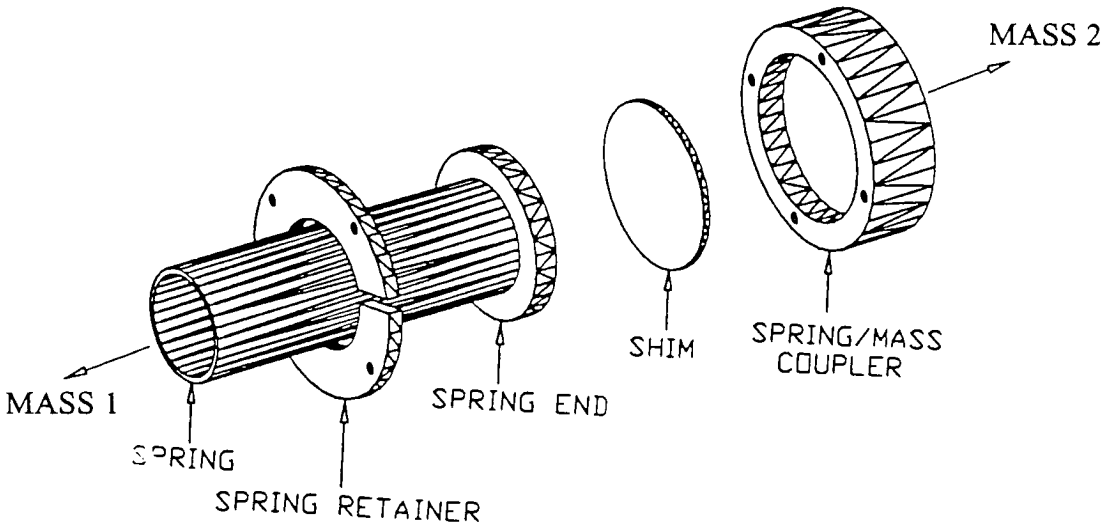

Figure 4-3

The spring/mass coupler is bolted through its center to the center of the mass (this is implied in Figure 4-1). This device allowed freeplay quantities to have a precision of ±.0002 inches with a high factor of repeatability. This was accomplished through the use of three shims, varying in thickness. The first set of shims allowed freeplay settings of .0000, .0010, and .0030 inches. The difference in response between .0010 and .0030 inches was immense. It was found that at .0030 inches, so much power was required to drive the system, that it was feared the equipment's power ratings would be exceeded. The system did, however, operate well with .0010 inches of freeplay present. A shim allowing freeplay of .0005 inches was examined and the differences in frequency response, between the three freeplay settings was substantial. This lead to the decision that these shims would be sufficient for the experiment. There was some concern

expressed as to what effect the shim would have if it were allowed to rattle around inside the freeplay device. To eliminate this possibility each shim was secured in place with a fastener.

The system was driven by a shaker connected to the center of mass 1. The shaker was controlled by a Data Physics PC analyzer. The response of the system was measured using piezoelectric accelerometers and a PCB force gauge. This data was directly fed to the same Data Physics analyzer where it was recorded as the real and imaginary components of the accelerance FRF.

A model for FRF estimation is shown in Figure 4-4.

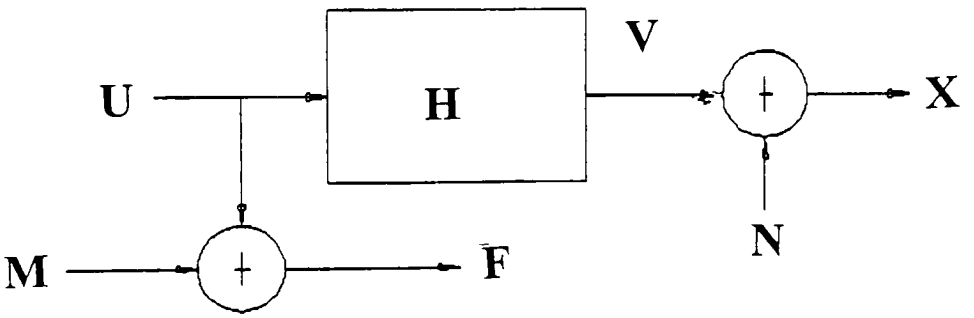

Figure 4-4 FRF model.

Where (F) is comprised of the true signal (U) and the noise signal (M), and (X) is comprised of the true output (V) and the noise signal (N), H represents the system.

The FRF is defined as [9]:

$$H_1 = FRF = \frac{G_{FX}}{G_{FF}} \tag{4.1}$$

$$\begin{aligned} G_{FX} &= FX^* \,(\, input \times conjugate\ of\ output) \\ G_{FF} &= FF^* \,(\, input \times conjugate\ of\ input) \end{aligned} \tag{4.2}$$

The FRF can be used to represent the amplitude of the system response at any frequency. Coherence is defined as:

$$\gamma^2_{XF} = \frac{|G_{XF}|^2}{G_{XX}G_{FF}} \tag{4.3}$$

$$\begin{aligned} G_{XF} &= XF^* \,(\, output \times conjugate\ of\ input\,) \\ G_{XX} &= XX^* \,(output \times conjugate\ of\ output\,) \\ G_{FF} &= FF^* \,(input \times conjugate\ of\ input\,) \end{aligned} \tag{4.4}$$

The coherence represents the quality of an average of the system response to a frequency. A coherence of 1 is a perfectly repeated signal (excellent signal quality), the number decreases to 0 as the signal quality decreases.

A step-sine program used in conjunction with the analyzer was used to excite the system. It was determined that a step-sine would be best method of excitation for this system due to the high signal-to-noise ratio and high coherence associated with the step-sine. The step-sine excites the system with a sine of one frequency until a certain criteria

is met. In this case the criteria was that either eight averages of the response be taken or the coherence of two or more signals exceeded 99%. When the criteria is met the step-sine will 'step up' an amount defined by the user to the next frequency. This continues until the set range of frequencies has been completely stepped through. The increments used in this experiment were .2 Hz through a range of 65 to 165 Hz. The system was cycled through the entire frequency range three times for each freeplay setting, once each for an input power rating of .5 mV, 2 mV, and 5 mV.

During the first run of the system with freeplay present, there proved to be a problem with out-of-plane vibrations near resonance. In addition to the vibrations in the linear direction (x) there were significant vibrations in the orthogonal (z) direction. This out-of-plane vibration was the result of the freeplay joint allowing the spring to influence the mass at points other than its center. This would induce moments into the system causing undesirable amounts of lateral motion. To eliminate the out-of-plane vibration the masses were secured in the lateral (z) direction through the use of nylon string. The string confined the motion of the masses to the linear direction (x). There was no noticeable up and down (y) direction motion and therefore was not of concern.

The method used to confine the masses can be seen in Figure 4-5.

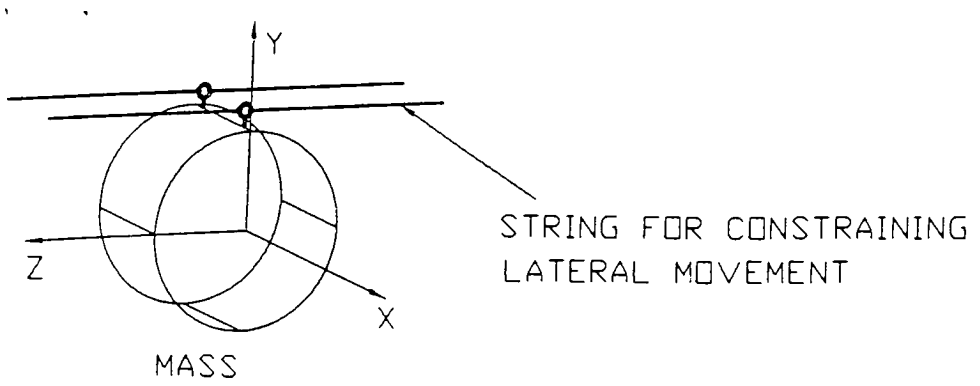

Figure 4-5

Once the system was perfected, the data was recorded and transferred to a modal analysis program. The initial plan was to use SMS Star but after analyzing the first couple cycles with freeplay, it was discovered that this would not be effective. SMS Star was unable to show the phase complexity this experiment was designed to examine; the problem being that SMS Star assumes the structure to be linear. Therefore a custom program had to be written to examine the system responses; this program is discussed in Appendix A. The program uses the circle fitting technique described in Section 3 to determine the system parameters. Through a moderate amount of user interaction the new program could be used to extract the information being sought.

5 Results:

5.1 Test Configurations for a Three Mass System:

For the three mass system pictured in Figure 4-1 and modeled in Figure 2.1-2 the following test configurations were used.

$$M_1 = M_2 = M_3 = 25 \text{ lbs}$$

$$K_1 = K_2 = 20{,}000 \text{ lbs/in}$$

Table I: Test configurations

Input power setting	gap size	spring with gap (spring 1 or spring 2)
.5 mV	.0005 inches	1
.5 mV	.0005 inches	2
.5 mV	.001 inches	1
.5 mV	.001 inches	2
2 mV	0 inches	neither
2 mV	.0005 inches	1
2 mV	.0005 inches	2
2 mV	.001 inches	1
2 mV	.001 inches	2
5 mV	.0005 inches	1
5 mV	.0005 inches	2
5 mV	.001 inches	1
5 mV	.001 inches	2

5.2 Data Analysis:

The system was run in each of the test configuration given in Table 1. For each configuration, the FRF of each mass response was recorded as its real and imaginary components. The plots of the FRFs allowed some insight as to the non-linear aspects of the system, these will be discussed in Section 5.3. The system parameters were able to be

extracted from the FRF data using circle fit parameter extraction methods. The theory behind the circle fit parameter extraction is discussed in Section 2.3 and the circle fit procedure is discussed in Section 3. Through observation of the trends of the extracted parameters, ω_n, ζ and A versus freeplay and versus power, a number of determinations were able to be made regarding this particular system's responses.

Each statement is followed by a supporting figure. Each figure represents the parameters of the first mass, first mode. For the trends involving freeplay the power applied was constant at 2 mV. All of the following trend plots are for X_1 and F_1, which is the driving point of the system. The driving point was the only response examined to simplify the results in a meaningful survey. There are other trends which are not shown due to the determination that they offered no significant contribution to the analysis. As indicated in the test configuration table, the system was measured for every combination of three different power settings, three different freeplay settings, and two different locations of freeplay. Each test run took two hours to complete.

- Increases in freeplay result in increases in modal complexity

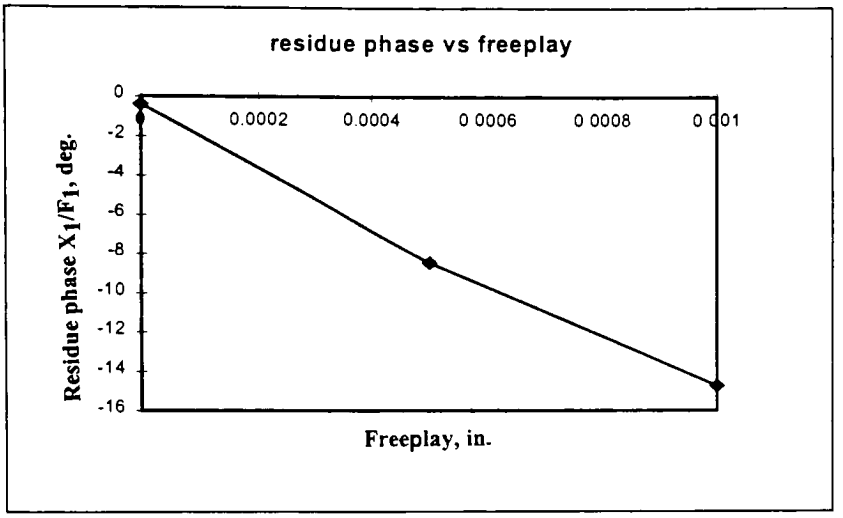

Figure 5.2-1

Every mode shape is made up of coordinates containing a magnitude and a phase angle. An ideal system will have real mode shapes with phase angles of 0 or 180°. Systems with proportional damping will also have real modes but the phase between the force and responses may be other than 0 or 180°. This is a real mode because even though the response is phase shifted from the input force, all the structural responses are in phase with each other. A system containing nonlinearities, such as nonproportional damping, friction, or gaps will have complex mode shapes. Nonlinearities in a system will result in time-varying mode shapes because each structural degree of freedom is independently phase-shifted from the force [2].

- Increases in freeplay result in increases in magnitude of the residue (modal amplitude)

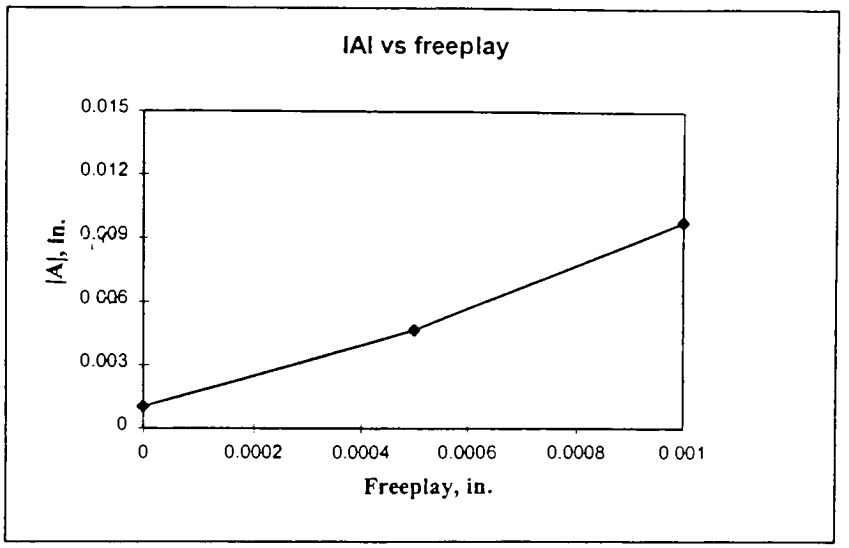

Figure 5.2-2

- Increases in freeplay result in decreases in the natural frequency

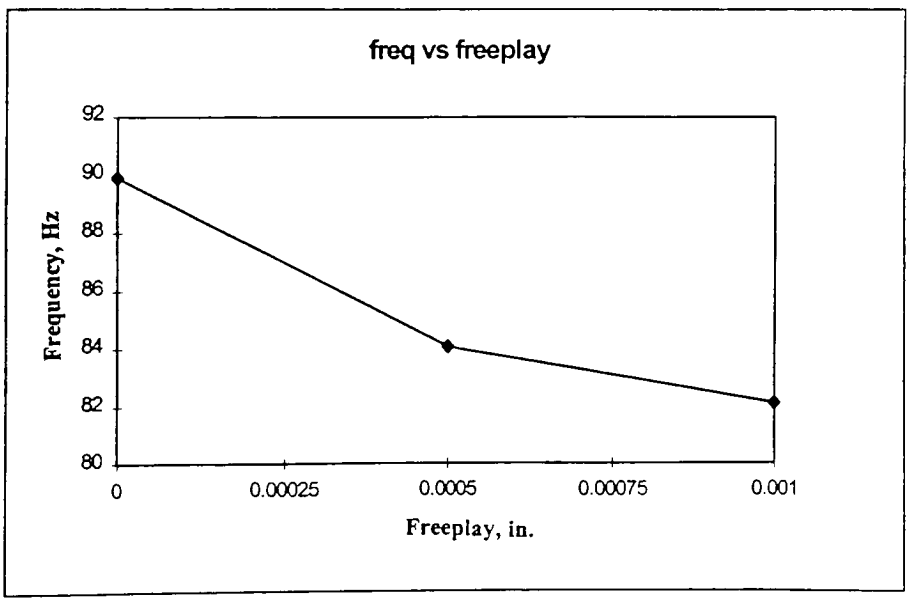

Figure 5.2-3

- Increases in freeplay result in decreases in the damping (due to irregular data points, the damping values are subject to suspicion)

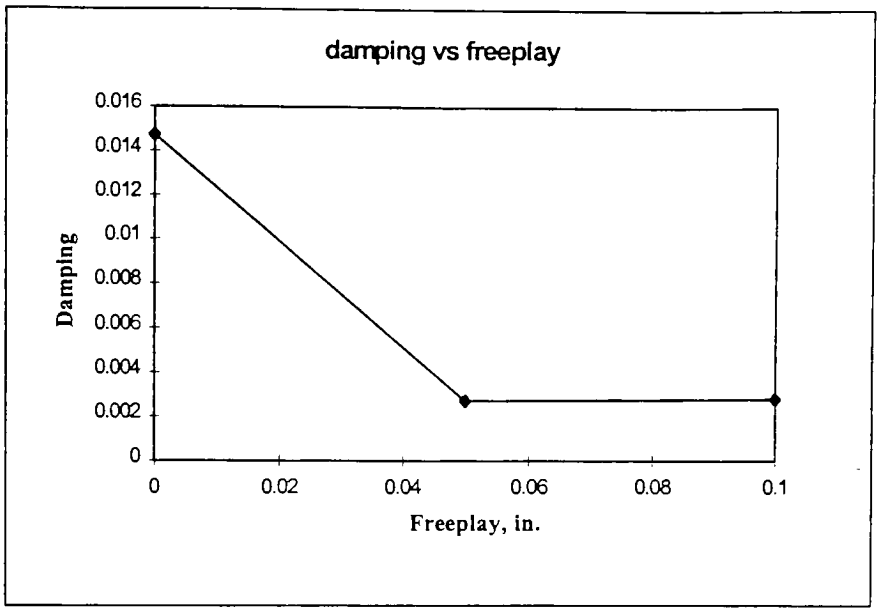

Figure 5.2-4

- Increases in power result in decreases in modal complexity

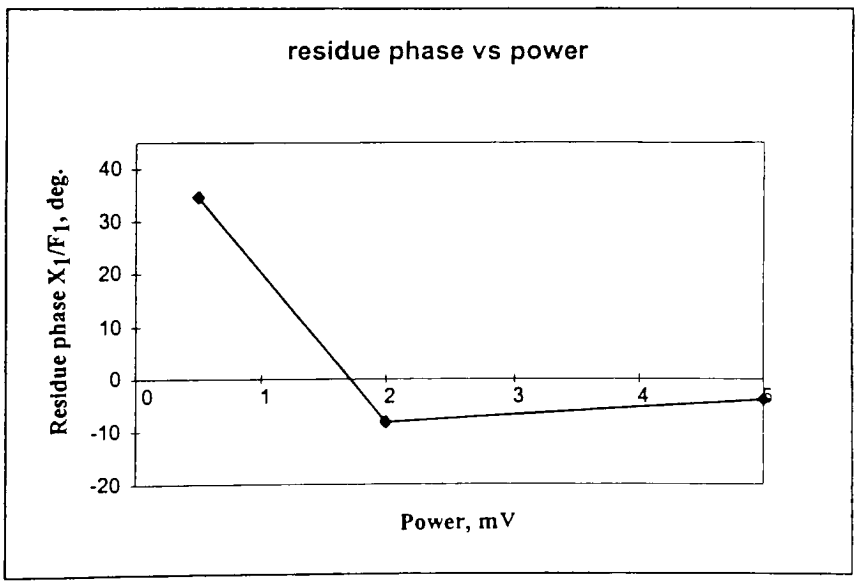

Figure 5.2-5

- Increases in power result in little change in magnitude of residue (modal amplitude)

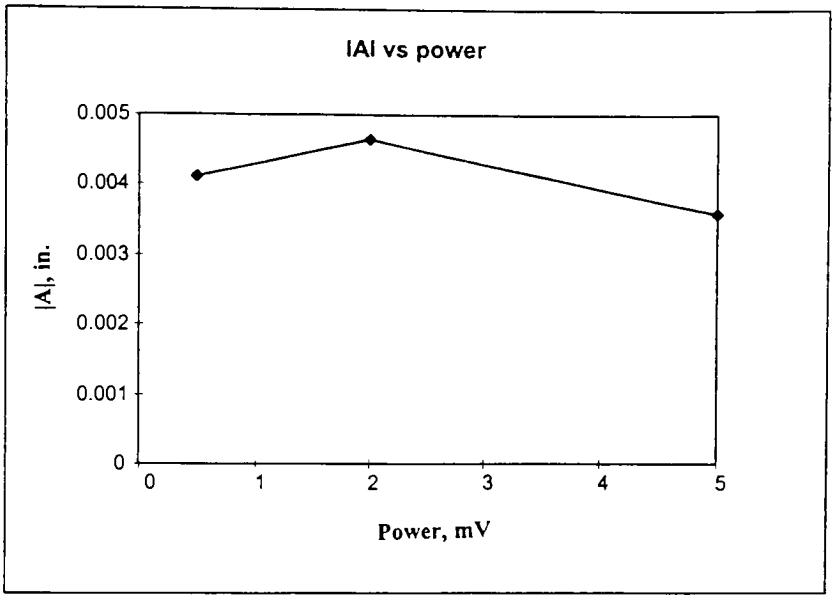

Figure 5.2-6

- Increases in power result in little change in the natural frequency

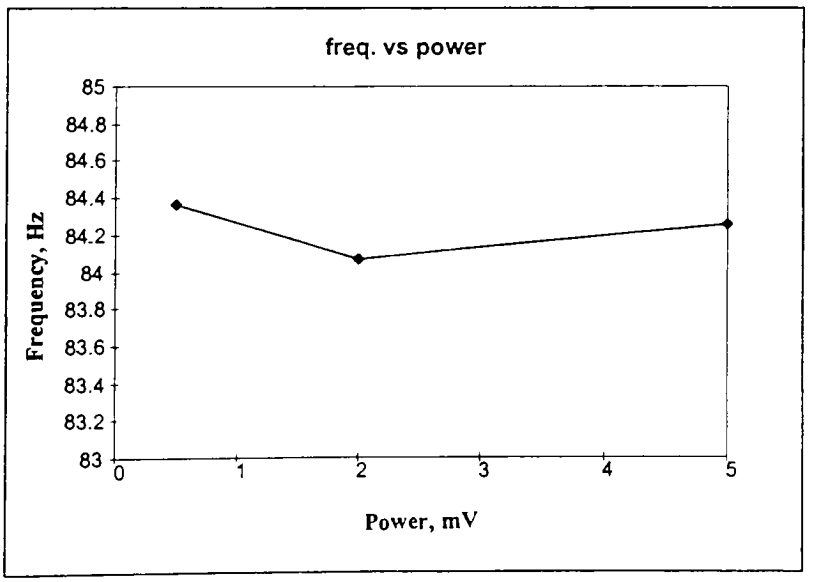

Figure 5.2-7

- Increases in power from .5 mV to 2 mV results in a decrease in damping, further increase in power to 5 mV results in an increase in damping (due to irregular data point, the damping values are subject to suspicion)

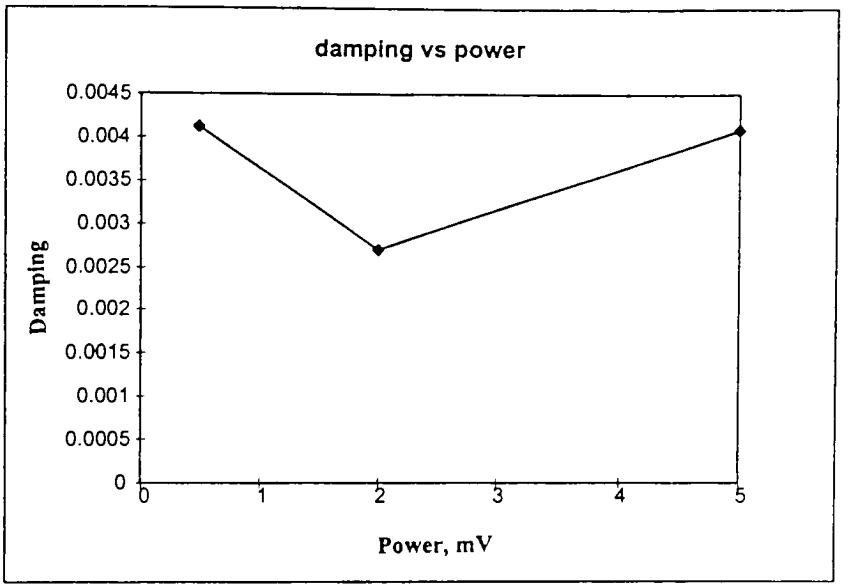

Figure 5.2-8

5.3 Nonlinear Dynamics in Frequency Domain

The results of the experiment were studied in several different graphing and 'fit' configurations. The frequency response functions (FRF) displayed some interesting characteristics of the system. A typical linear FRF with light damping would show a degree of symmetry around a vertical line drawn through the natural frequency. Several of the FRF plots (not shown) for the system with freeplay displayed behaviors near the resonant frequency called jump phenomena [9] (recall the jump phenomena is a sudden rise or drop in frequency response, from Section 2.3). Measured plots of the observed jump phenomena can be seen in Figure 5.3-1 (these plots are generated from actual testing of the system shown in Figure 4-1 and the test configurations discussed in Sections 5.1 and 5.2).

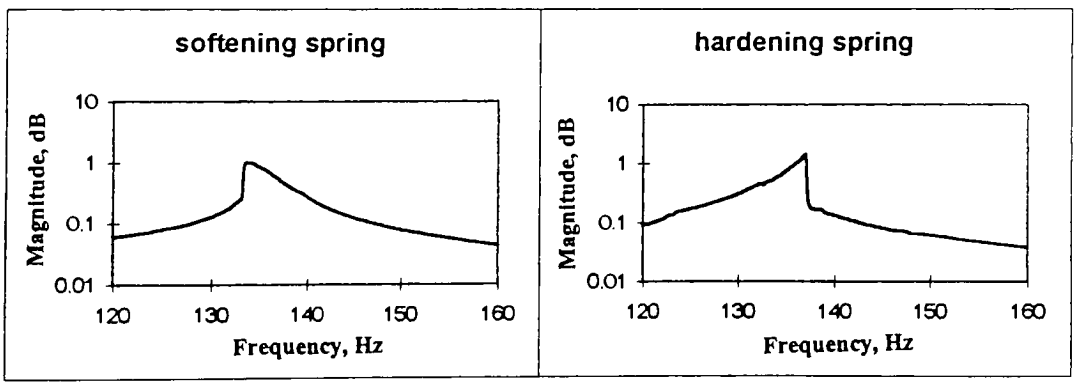

Figure 5.3-1(a) FRF of softening spring, (b) hardening spring

The freeplay in the system creates the appearance of a spring with cubic stiffness, it also introduces coulomb friction into the system. The cubic stiffness can give the appearance of either a hardening or softening spring while the coulomb friction will tend

to give the appearance of a softening spring. The appearance of cubic stiffness is due to two distinct spring stiffnesses experienced as the system cycles. There is one stiffness as the spring passes through the region of freeplay (gap) and another stiffness when the spring is in contact with the mass on either side of the gap. The only stiffness experienced in the gap is caused by the small amount of coulomb friction between the slider and the guide; the stiffness is very small. Figure 5.3-2 is a representation of the stiffness experienced by the system for one half cycle.

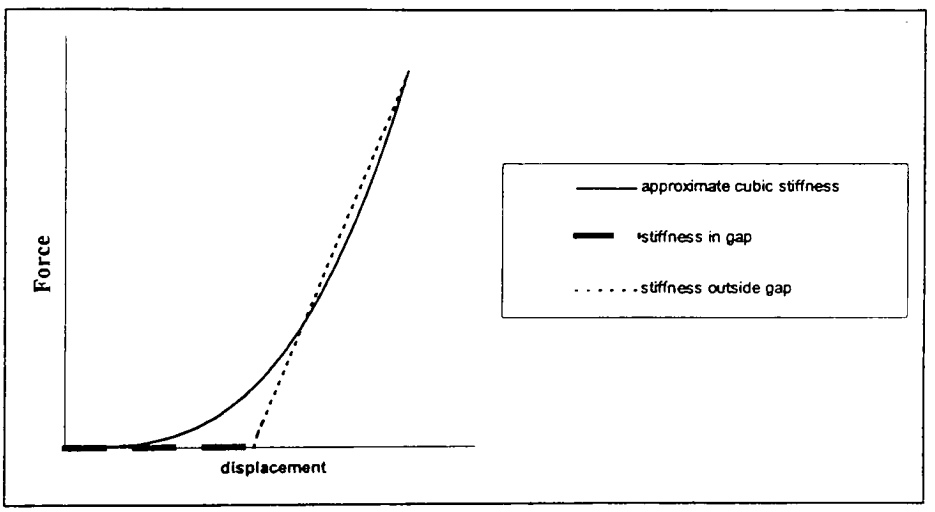

Figure 5.3-2 curves representing the stiffness in system for one half cycle.

The characteristics of the system with freeplay can be altered between showing a hardening or softening spring by changing the power applied to the system or the amount of freeplay present. This can be proven through the development of a few equations which will result in an approximation of the basic equation of motion for this system.

Recall the basic equation of motion with coulomb friction present(2.43):

$$F = M\ddot{x} + C\dot{x} + Kx + \mu N \tag{2.43}$$

where μ is the coefficient of friction and N is the normal force experienced at the point where friction occurs. Some conditions need to be applied to equation (2.43) for the freeplay system:

$$F = M\ddot{x} + C\dot{x} + Kx + \mu N \begin{cases} \mu N = \mu N; \text{condition A} \\ \mu N = 0; \text{condition B} \end{cases} \tag{5.1}$$

Condition A is only in effect for the distance, equal to the amount of freeplay, the system travels after reversing its direction upon reaching one of its travel extremes. Condition B is the total distance the system travels for one cycle, less the initial distance traveled through the gap. The limits need to be applied because the coulomb friction only influences the system for the short time that the spring is in the gap; when the spring is in contact with either side of the gap μN=0.

Recall the Duffing equation (2.42):

$$F = M\ddot{x} + C\dot{x} + Kx \pm \beta x^3 \tag{2.42}$$

Combining equations (2.42) and (5.1):

$$F - \mu N = M\ddot{x} + C\dot{x} + Kx + \beta(x)^3 \tag{5.2}$$

The same conditions as those for equations (5.1) apply to equation (5.2), they are not shown for reasons of simplicity.

With a basic understanding of equation (5.2), the response of the system can be anticipated for various initial conditions and various input signals. The system will be dominated by either coulomb friction or cubic stiffness depending on the amount of freeplay present, the amount of power driving the system, and the frequency at which the system is being excited. The domination of the system is a result of any one or combination of the following situations:

1. Motion through the gap. As the spring end passes through the gap, the system experiences coulomb friction.
2. Energy loss. Energy will be lost in the form of noise and heat each time the spring end contacts either end of the gap.
3. Discontinuity in stiffness. While the spring end is in the gap, the stiffness of the system is essentially 0 and when in contact with either end of the gap the stiffness increases to 20,000 lb/in.

At low power and small amounts of freeplay, the effects of coulomb friction (softening spring) will dominate the system response, as seen in Figure 5.3-3.a. As the power and or freeplay increase the cubic stiffness (hardening spring) will tend to dominate the system response, seen in Figure 5.3-3.b.

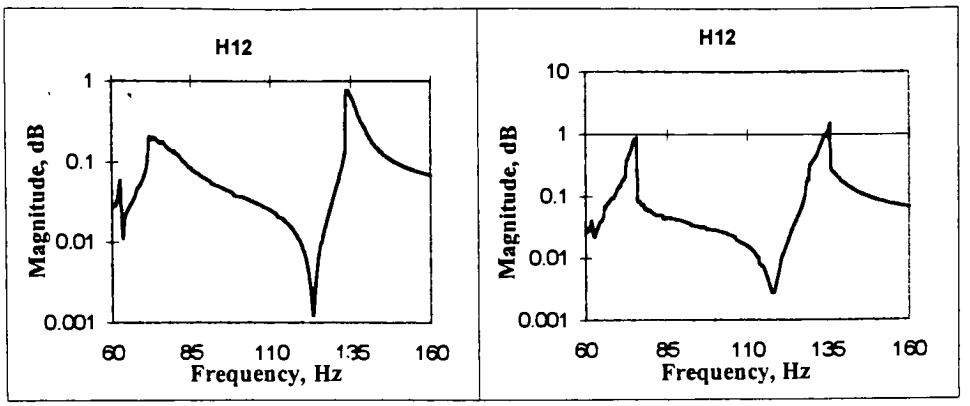

(a) (b)

Figure 5.3-3 (a) FRF of system dominated by coulomb friction, (b) FRF of system dominated by cubic stiffness.

The dominance of the system response by coulomb friction is the result of a combination of, a percentage of the input energy used to overcome the friction and the small amount of distance the spring travels through the gap. An increase in the power supplied, (force), and or an increase in freeplay will result in the apparent cubic stiffness of the spring dominating the system response. This is due to the apparent effects of the coulomb friction diminishing as the input power increases and the effects of the apparent cubic stiffness increasing as the amount of freeplay increases.

Occasions may arise when the cubic stiffness will dominate the first mode and the coulomb friction dominates the second mode. This would result in an FRF similar to Figure 5.3-4.

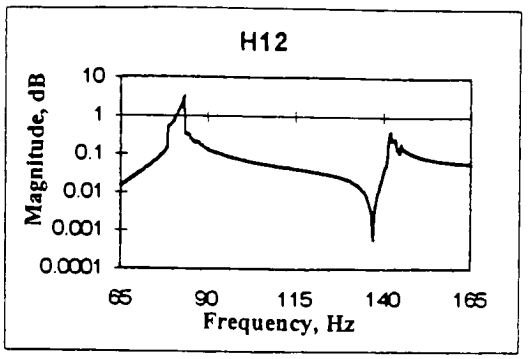

Figure 5.3-4 sample plot showing cubic stiffness dominated first mode and coulomb friction dominated second mode.

Here the power and freeplay are such that the cubic stiffness dominates the first mode but as the response frequency increases the effect of coulomb friction increases until it dominates the system response. This has been termed as the "dual spring condition."

The dual spring condition can be explained when the damping effects of coulomb friction are considered. It has been found for the freeplay system that the spring deflection for the first mode is greater than the deflection for the second mode. This can be observed in the FRFs of the system containing no freeplay or shown mathematically.

Recall equation (2.35):

$$\frac{X_i}{F_j} = \sum_{r=1}^{n} \left(\frac{\hat{\phi}_{ir} \hat{\phi}_{jr}}{-\omega^2 + i2\zeta\omega_r\omega + \omega_r^2} \right) \tag{2.35}$$

using system values found in Section 2 for ϕ and ω_r, equation (2.35) will show the total spring deflection per cycle.

For the first mode:

$$\frac{X_1 - X_2}{F_1} = \left(\frac{2.78^2}{i2\zeta(2\pi(88.48))^2} \right) - 0 = 1.25E-5/i\zeta$$

For the second mode

$$\frac{X_1 - X_2}{F_1} = \left(\frac{(-1.6)^2}{i2\zeta(2\pi(153.28))^2} \right) - \left(\frac{(-1.6)(3.2)}{i2\zeta(2\pi(153.28))^2} \right) = 1.38E-6/i\zeta$$

this indicates that the second mode spring travel is almost an order of magnitude less than the travel for the first mode.

Now consider that the coulomb damping is only a fraction of the total spring travel (cycle), and that the friction only effects the system while traveling through that fraction. The damping will be in effect for a greater percentage of the second mode cycle than it is in the first mode cycle. Therefore, if the power and freeplay settings are such that the first mode is dominated by cubic stiffness, the decrease in spring travel as the system nears the second mode may increase the effects of the coulomb friction to a point where it dominates the system response. This will allow the situation of a hardening first mode and a softening second mode to occur.

An additional factor to the coulomb friction dominated second mode is energy loss. From basic physics it is known that energy is a function of force.

Recall equation (5.2) with its conditions:

$$F - \mu N = M\ddot{x} + C\dot{x} + Kx + \beta(x)^3 \tag{5.2}$$

This equation demonstrates that the coulomb fiction is basically a drain on the energy being delivered to the system. Therefore, it is safe to assume that other energy losses would have effects similar to that of coulomb friction. Most of the time these losses would be small and negligible, but there may be occasion when the added energy loss is a significant factor. Energy loss may be a factor when the dual spring condition appears. As the system response frequency increases the energy loss as heat and noise will increase: this is caused by an increase in the pitch and volume of the spring rattling in the gap (noise), and the number of times/second the spring impacts either side of the gap (heat). This increase in energy loss could add to the softening effects already caused by the coulomb friction and aid in the dominance of the softening spring at the second mode.

A circle plot of the system with freeplay can also give insight as to whether a system is exhibiting hardening or softening spring characteristics. A circle plot of the system with freeplay will appear to be missing a portion of the circle. If the missing portion of the circle is in the negative region of the imaginary axis, the spring is hardening. If the missing portion is in the positive region of the imaginary axis, the spring is softening. These missing portions can be associated with the jump phenomena viewed in the FRFs, and occur for the same reason. A comparison of a Nyquist plot and an FRF plot, both showing hardening spring characteristics, is seen in Figure 5.3-5.

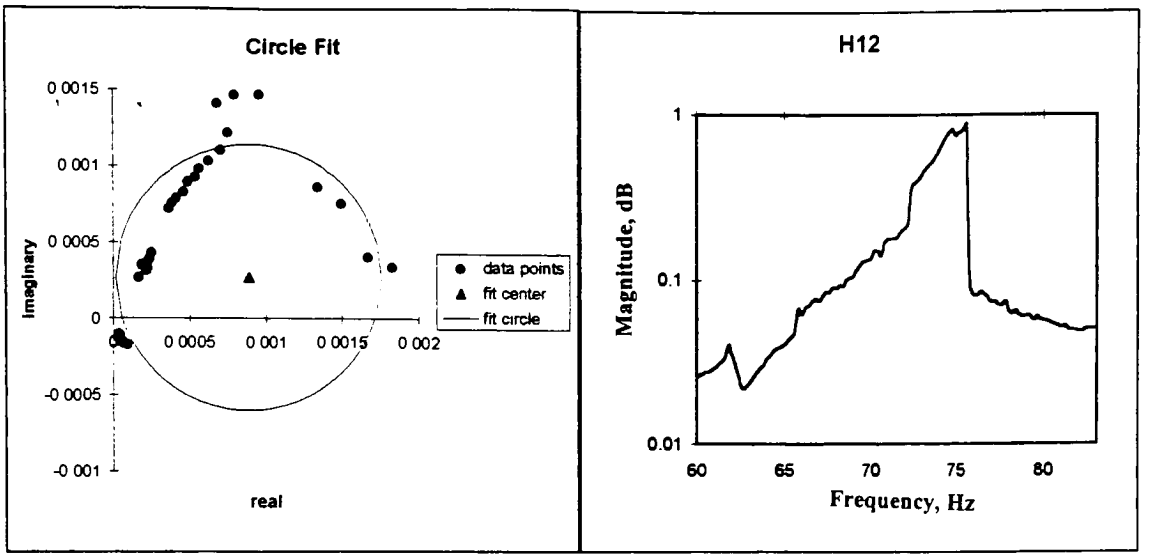

(a) (b)

Figure 5.3-5 (a)Nyquist plot showing hardening spring, (b) FRF showing hardening spring.

A comparison of a Nyquist plot and an FRF plot, both showing softening spring characteristics, is seen in Figure 5.3-6.

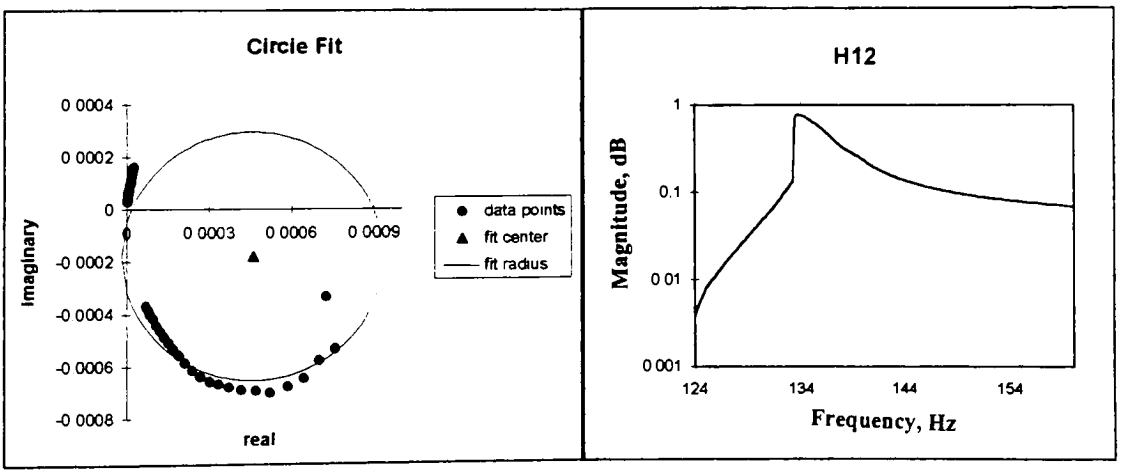

(a) (b)

Figure 5.3-6 (a)Nyquist plot showing softening spring, (b) FRF showing softening spring.

It may be noted at this point that the circle plots of Figures 5.3-5 and 5.3-6 do not 'fit' as well as the plot in Section 2.2, Figure 2.2-2; this is a direct result of the nonlinearities present in the system with freeplay. A plot of the distance that each data point varies from the fit circle, a variance plot, will indicate the degree of linearity of a system. Figure 5.3-7 is typical variance plot of a linear system, while Figure 5.3-8 is typical of the nonlinear system examined in this study.

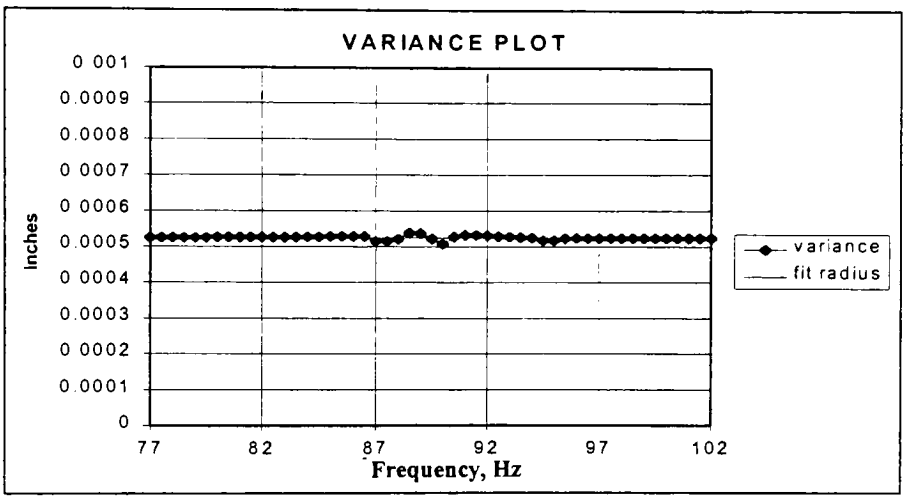

Figure 5.3-7

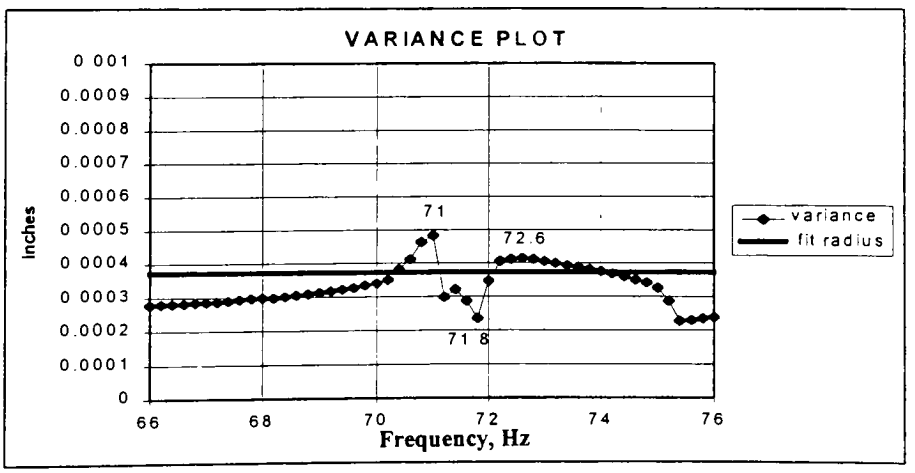

The valid data points of this system when linear will tend to have a variance of less than ±5%. With freeplay in the system, the data points will tend to trace an ellipse rather than a circle. For this system the ellipse will have a major axis parallel to the imaginary axis. It is typically along the curve of the minor axis that the frequency is located. This would be between the two peaks of the variance curve (between 71 and 72.6 Hz, for Figure 2.3-7). Where the natural frequency fell within the valley, was not found to be of significance.

Figures 5.3-9 and 5.3-10 show the trends of variance with respect to freeplay and power respectively.

- Increases in freeplay result in increases in the variance.

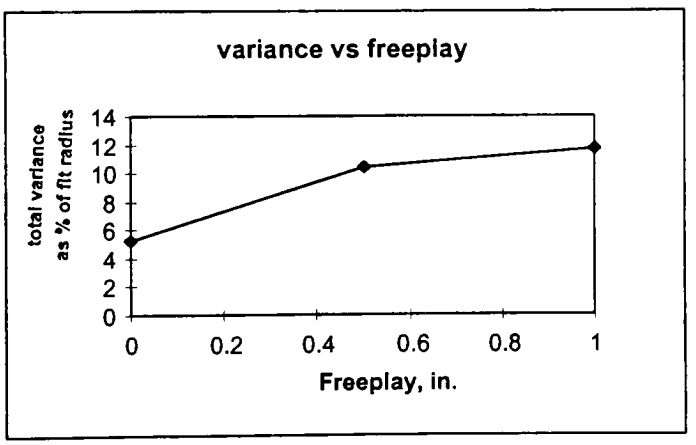

Figure 5.3-9

- Increases in power result in first, a decrease in variance towards linearity and then an increase in variance away from linearity (this occurred only for small amounts of freeplay.

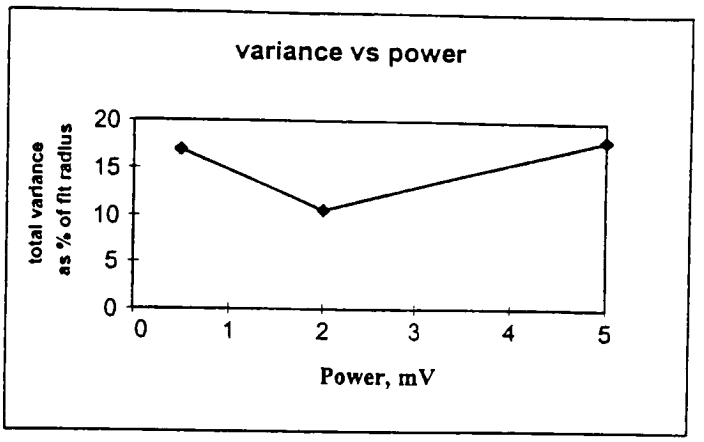

Figure 5.3-10

As expected, the degree of nonlinearity of the system increases as the amount of freeplay increases. The trend of variance versus power may be a little surprising at first. What happens is easily explained. At .5 mV power input, the system is dominated by the coulomb friction as the power is increased to 2 mV, the effects of coulomb friction diminish until the cubic stiffness dominates the system. The trend toward linearity is the direct result of the softening effects of coulomb friction and the hardening effects of cubic stiffness acting to cancel each other out. This would result in the system reacting as if it had neither softening nor hardening spring characteristics. Further increases in power result in further dominance of the system by cubic stiffness.

The variance data proved to be useful in the detection of freeplay and the FRFs proved to be useful in determining the type of nonlinearity (cubic stiffness or coulomb friction) dominating the system.

6 Conclusions and Recommendations:

An investigation into the effects of freeplay was undertaken. A three mass, two spring system with adjustable amounts of freeplay was studied, resulting in the modal parameter trends shown in Table II.

Table II: Test Results

Parameter	Increasing freeplay	Increasing power
ω_n	decreases	remains fairly consistent
ζ	decreases (unreliable)	decreases then increases (unreliable)
Residue phase	increases	decreases
$\|A\|$	increases	remains fairly consistent
Variance	increases	decreases then increases

It was found that freeplay in a system will induce coulomb friction and the appearance of cubic stiffness. These are most identifiable in the FRFs as the appearance of the jump phenomena, indicating hardening or softening springs, as described by Duffing's equation. Modal parameters were extracted using a circle fit technique and then studied for trends as plots of the system parameters versus power and system parameters versus freeplay.

It is indicated by the parameter trends that the effect of different power levels has varied effects on the parameters. Low input power resulted in high degrees of modal complexity which would decrease as the power was increased. As the power increased, the linearity of the system decreased to a point and then started increasing again.

The effects of varying amounts of freeplay appeared to be more predictable.

Increases in freeplay resulted in modal complexity, along with other parameters, consistently increasing or decreasing.

The FRF can indicate whether the system is dominated by coulomb friction or cubic stiffness. This can be a fair indicator as to the amount of freeplay in the system. The larger the amount of freeplay the larger the jump indicating a hardening spring. This method is not ideal for indicating freeplay, in that the jump can get quite small (almost undetectable) as the system domination switches from softening to hardening spring characteristics.

A better method of determining freeplay is the variance plot. The variance plot is a plot representing the distance each data point is from the best fit circle. For this particular system a typical linear response will have a small amount of variance, approximately less than ±5% of the fit radius. The variance is a reliable indication of nonlinearity, it was found that as the nonlinearity increases so did the variance. This relationship allows the variance to be a reliable indicator of freeplay, as the freeplay increases so does the nonlinearity.

Better methods of estimating the damping is needed to determine the effect of freeplay on damping. The current method described in Section 4 results in a scatter of damping estimates (some up to 50% standard deviation) near the natural frequency due to the non-linearities in the system.

It is recommended that future studies of freeplay using this type of system concentrate on varying the amounts of freeplay. It is apparent that the system is very

sensitive to the amount of freeplay. Gaul, Lenz, and Sachau's [5] paper on joint stiffness indicates that a system's response may be effected by inperceivable amounts of freeplay. A more precise method of inducing freeplay must be designed and the system needs to be cycled using more freeplay settings with a constant power setting.

References

[1] Alexander, R.M., Noah, S.T., and Franck, C.G., "Parametric Identification of a Vibratory System With a Clearance," *Journal of Vibration and Acoustics*, Vol. 115, pp. 25-31, January 1993.

[2] Berg, J., 'Rapid Modal Analysis for Large Nonlinear Structures,' Omicon Corp., San Diego, CA proposal pp. 1-20. July 1995.

[3] Chattopadhyay, S. And Saxena, R., "Dynamics of a Loosely Restrained Structure," *ASME Winter Annual Meeting,* December 1-6, 1991.

[4] Ewins, D.J., "Modal Testing: Theory and Practice," England, Research Studies Press Ltd. 1985.

[5] Gaul, L., Lenz, J., and Sachau, D., "Active Damping of Space Structure by Contact Pressure Control in Joint," *Proceedings of the First International Modal Analysis Conference* 1997 pp. 202-208.

[6] Hsu, S.T., Griffin, J.H., and Bielak, J., "How Gravity and Joint Scaling Affect Dynamic Response," *AIAA Journal*, Vol. 27, 1989. pp. 1280-1287.

[7] Kochersberger K., "Experimental Modal Analysis: Theory and Application," Department of Mechanical Engineering, Rochester Institute of Technology, Rochester, NY class notes, Spring 1996.

[8] Masri, S.F., "Analytical and Experimental Studies of a Dynamic System With a Gap," *Transactions of the ASME / Journal of Mechanical Design*, Vol. 100, July 1978 pp. 480-485

[9] McConnell, Kenneth G., "Vibration Testing," New York, John Whiley and Sons, Inc. 1995.

[10] Menq, C.H., Bielak, J. And Griffin, J.H., 'The Influence of Microslip on Vibratory Response, Part I: A New Microslip Model," *journal of Sound and Vibration*, Vol. 107, June 1986, pp. 279-293.

[11] Menq, C.H., Bielak, J. And Griffin, J.H., 'The Influence of Microslip on Vibratory Response, Part II: A Comparison With Experimental Results," *journal of Sound and Vibration*, Vol. 107, June 1986, pp. 295-307.

[12] Moon, F.C. and Li, G.X., "Experimental Study of Chaotic Vibrations in a Pin-Jointed Space Structure," *AIAA Journal*, Vol. 28, May 1990, pp. 915-921.

[13] Richardson, Mark H. And Formenti, David L., "Parameter Estimation From Frequency Response Measurements Using Rational Fractional Polynomials," *Proceedings of the First International Modal Analysis Conference* 1982 pp. 167-181.

Appendix A :

Use of the EXCEL Spread Sheet, Curve Fit and Parameter Extraction Program

The program is designed for extracting the modal parameters of a harmonic system. The program is designed to accept 501 data points with a minimum of 51 data points per mode; the data points must be the real and imaginary components of the accelerance FRF. The program will accept up to 3 transfer functions, H12, H13, and H14.

1. Go to the sheet labeled 'FRF'
2. Under the heading 'Freeplay' define the frequency range to be examined.
3. For H12, H13, or H14 enter the real and imaginary accelerance data points in the appropriate column.
4. FRFs of the data may now be viewed at the bottom of sheet 'FRF'
5. Name the 51 points to be used for the analysis; 25 points above the suspected natural frequency, 25 points below the suspected natural frequency, and the suspected natural frequency. The suspected natural frequency can be determined from the frequency of maximum altitude from the respective FRF.
6. Name the real and imaginary data points, corresponding to the previously named frequency values, as a 2x51 matrix.
7. Change active sheet to 'fit'; interactive cell are highlighted in yellow.
8. Set the 51 cells below the heading 'frequency' equal to the name defined in step 5. This is done by highlighting the 51 cell and typing ="NAME" CTRL+SHIFT+ENTER.

9. Set the 102 cells, a 2x51 matrix, below the headings 'real' and 'imaginary' equal to the name defined in step 6. Use same method described in step 8.
10. To determine the data points to be used for the circle fit, go to the cells below the heading 'acceptable data points' While viewing the circle plot and using a trial and error method insert values into 'above real value', 'below real value', and 'above imaginary value' until the desired points for the fit are properly shown on the plot.
    - Above real data is the value that the real value of the data point must be greater than to be plotted. Below real data is the value that the real value of the data point must be less than to be plotted. Above imaginary data point is an override value; any data point that has an imaginary value greater than this will be plotted regardless of what the value for above or below real value is.
11. Enter initial guesses for the circle radius and (X,Y) location. These are entered under their appropriate subheadings under the heading 'FIT CIRCLE'
12. Run the Excel solver; minimizing the target cell (target) by changing the cells under radius, X, and Y (rd, f, and b respectively).
13. Once the solver arrives at a solution, copy the values for the radius and (X,Y) location under the heading 'fit circle information' This will be useful when examining several masses or modes.
14. Change the active sheet to 'circfit'; interactive cell are highlighted in yellow.

15. The plot in 'dθ/dω max' represents the rate of change of sweep for the data points around the circle. The highest point in this plot represents the maximum rate of change; enter this points label into the cell below the heading 'max'

    - The label of the maximum point should be located between rows 27 and 35, the green rows. If the point does not fall into this range there is a problem somewhere. Check the value in the cell below the label f_n, this is next to 'max' This value should be within 2-3 values of the suspected natural frequency of step 5, if it is then there was a mistake made when naming the selected frequency range. Start again at step 5 using the value of f_n as your suspected natural frequency. If f_n is not near the suspected natural frequency there may be irregular data points effecting the data. Select a local maxima that has a label which falls between 27 and 35; the higher the peak the better.

16. Once a valid maxima is entered into the cell below 'max' highlight 5 values in the red bordered section in column K; values from 2 above the local maxima to 2 below the local maxima. Paste these values, using 'paste special-values', into the column under 'max finder'-'dθ/dω'; the plot titled 'max magnified' will be automatically updated.

    - The plot of 'max magnified' is zoomed view of the maxima seen in plot 'dθ/dω max' A trendline has been fit to these points and the equation for the trend line should be seen in the plot. If the equation is not seen;

reformat the trendline so that the equation is not displayed on the plot and then reformat it so that the equation is displayed on the plot.

17. Enter the trendline equation into the cell below the heading 'max finder'-'solver'
18. Run the Excel solver; maximizing the target cell (E) by changing cell X (x).
19. Once the solver has arrived at a solution copy the value of X into the corresponding column under the heading 'local maximums'; column 11 for mass1 mode1, column 12 for mass1 mode2, column 21 for mass2 mode1, and so on.
20. Enter the mass/mode number into the cell to the right of the cell titled 'mass/mode' using the same numbering scheme described in step 19; 11, 12, 21, ect.
21. All plots now represent the system in question. Circle plot can be viewed in sheet 'fit', Variance plot can be viewed in sheet 'circfit', FRF plots are viewed in sheet 'FRF', and the Damping plot can be viewed in sheet 'results'. The system parameters can also be seen in sheet.